JPhys Energy

TOPICAL REVIEW • OPEN ACCESS

Harnessing the unique properties of MXenes for advanced rechargeable batteries

Journal of Physics: Energy

TOPICAL REVIEW

Harnessing the unique properties of MXenes for advanced rechargeable batteries

Deobrat Singh[1,2], **Vivekanand Shukla**[2,3], **Nabil Khossossi**[1,2,4], **Abdelmajid Ainane**[1,4] and **Rajeev Ahuja**[1,5]

[1] Condensed Matter Theory Group, Materials Theory Division, Department of Physics and Astronomy, Uppsala University, Box 516, 75120 Uppsala, Sweden
[2] Department of Microtechnology and Nanoscience (MC2), Chalmers University of Technology, SE-412 96 Gothenburg, Sweden
[3] Laboratoire de Physique des Matériaux et Modélisations des Systémes, (LP2MS), Unité Associée au CNRST-URAC 08, Faculty of Sciences, Department of Physics, Moulay Ismail University, Meknes, Morocco
[4] Applied Materials Physics, Department of Materials Science and Engineering, Royal Institute of Technology (KTH), S-100 44 Stockholm, Sweden
[5] These authors contributed equally to this work.

E-mail: rajeev.ahuja@physics.uu.se

OPEN ACCESS

RECEIVED
2 June 2020

REVISED
21 October 2020

ACCEPTED FOR PUBLICATION
27 November 2020

PUBLISHED
18 December 2020

Keyword: MXene, rechargable batteries, metal-ion batteries, lithium–sulfur (Li–S) batteries, two-dimensional (2D) materials, Van der Waals heterostructure

Abstract

In recent years, two-dimensional MXenes have been emerged as potential electrode materials for rechargeable batteries due to their unique properties such as exceptional safety, significant interlayer spacing, environmental flexibility, large surface area, high electrical conductivity, and excellent thermal stability. This review examined all of the recent advances in the field of MXenes and their composites (hybrid structures), which are found to be useful for the electrochemical applications of advanced rechargeable batteries. The main focus of this review is on metal-ion batteries and lithium–sulfur (Li–S) batteries. It is intended to show that the combination of recent improvements in the synthesis and characterization, greater control of the interlayer distance, and new MXene composites, together serve as an emerging and potential way for energy storage applications.

1. Introduction

Since the isolation of graphene in 2004, the importance of two-dimensional (2D) graphene-like materials has been growing significantly in the scientific community owing to their outstanding features such as excellent mechanical, electronic, and optical properties, and their exciting potential for various practical applications. Given their high surface-to-volume ratio, 2D materials (2DMs) offer high specific surface areas to enable full utilization of all accessible sites as effective electrode materials. As a result, the exposed contact area is significantly enhanced within the electrodes and electrolytes, and also the pathways for the transport of charges are reduced. These characteristics of excellent electrochemical properties make them suitable candidates for various energy storage applications. The key appeal of 2DM is the property that makes them naturally suited for a type of integration that is not so much possible with any three-dimensional (3D) material, forming heterostructures by stacking 2DMs together in the form of lateral vertical device, doping flexibility, nanoconstrictions, and several others. Over the last decade, a considerable research has been carried in identifying new 2DMs, mainly by focusing on mono elemental and those containing double elements such as, graphene, [1] silicene, [2] germanene, [3] phosphorene, [4] transition metal dichalcogenides (TMD), [5] transition metal oxides (TMD) [6]. Among the family of 2DMs beyond graphene, transition-metal carbides, carbonitrides, and nitrides also called MXenes materials [7–12] have attracted munch interest. Their general chemical formula is $M_{n+1}X_nT_x$ with $n = 1$, 2, 3 or 4, where M is Transition-metal, X represents carbon and/or Nitrogen-atom, and T is hydroxyl (OH), oxygen (O), or fluorine (F) [13–15]. The transition-metal carbide $Ti_3C_2T_x$ was the first 2D MXene successfully synthesized

using aqueous fluoride-containing acidic solution to etch down to a few layer and further exfoliated with water and other organic solutions in 2011 [7]. $Ti_3C_2T_x$ manifested unique structural and electronic properties in both the experiments and theoretical modeling. A year after this ground-breaking research, universal etching of Al from many other MAX phases gave rise to the new family of 2DMs known as MXenes. Until now numerous MXenes have been successfully synthesized, including 2D Vanadium Carbide ($V_{n+1}X_nT_x$) [16] and Niobium Carbide ($Nb_{n+1}X_nT_x$) [17]. It has become the broadest category of 2DMs and is still growing significantly due to the range of various elemental configurations and prospective applications [18–23]. Their exciting properties and utilization in number of applications have been reported in various published reviews recently [24–30].

Motivated from the stimulating properties and suitability in energy storage application, in this review, we would focus on alkali-ion and unexplored Li–S batteries electrode applications of pristine phases and heterostructures of MXenes. We start by introducing the family of the layered MAX phases with the aim of better understanding of the MXenes and their synthesis with the various functional groups such as oxygen (–O), hydroxyl (–OH) and/or fluorine (–F). We would simultaneously focus on the importance of computational design of MXenes in the prediction of new members of the family and their heterostructures, as well as toward the better understanding of their physical and chemical properties at an atomic-scale (section 2). In sections 3 and 4, we outline recent cutting edge works related to the development of MXene with enhanced performance for rechargeable battery electrode applications such as lithium-ion, non-lithium ion, and lithium-sulfur batteries. We will review the effect their surface functionalization and heterostructure in order to achieve high storage capacity and high safety battery performance, focusing on physical and chemical characterization, computational modeling, and electrochemical properties. Finally, section 5 is dedicated to summary and highlighting the critical challenges in developing MXene and their heterostructures for alkali-ion and Li–S battery applications.

2. MXenes: structure, synthesis and properties

2.1. Structure

In 1960s, hundreds of new carbides and nitrides were identified by Hans *et al* in Vienna [31], but these phases remained unexplored for nearly 30 years until 1990s. Later Barsoum and El-Raghy synthesized Ti_3SiC_2, which showed remarkable electronic and thermal conductivity with a suitable combination of ceramic and metallic properties [32]. Further, synthesis of Ti_4AlN_3 suggested that these phases shared a basic structure, which was later designated the acronym '$M_{n+1}AX_n$ phases' ($n = 1, 2, 3$, etc) or 'MAX phases'. M is a transition metal (mostly group 13 and 14 elements), A stands for group IIIA or IVA elements, and X is C/N [33, 34]. The MAX phases constitute a significant group of currently > 130 diverse compositions, vast majority of which crystallizes in hexagonal structure with the *P63/mmc* space group or other derivatives [35]. Figure 1 shows the schematic crystal structures of MAX phase materials. The structure is comprised of MX_6 octahedra, with pure Al layers. The main difference separating these three different MAX phases, viz. $n = 1$, 2, or 3, is in the number of M layers (2–4) between the A layers. They are assigned as 211, 312, and 413, sequentially [36–38].

The exposure of the chemically active exterior metals layer of a MAX phase causes surface terminations. This further can remove the 'A' element from the bulk MAX phases and result in the mono or few layers of MXene, which is described in figure 1. The schematic picture of 2D-MXenes consist of different variants of monolayers. M_2X is the tri-sublayer structure, where the carbon/nitrogen (X) atom is sandwiched in between two metal (M) atom layers in a hexagonal unit cell. There are also M_3X_2 and M_4X_3 sheets, as shown in figure 1. Besides these, there are possibilities of double transition metal MXenes. This contains a sandwiched configuration of X between two different transition metals 'M and M', and these metals can be randomly distributed [11, 39, 40]. It is well understood that outer metal atoms would play a vital role in deciding the surface behavior of these MXenes. Since the metal atom generally has coordination number six, it is quite natural to expect that the transition metals in MXenes favor making six chemical bonds with the neighboring atoms [41, 42]. Hence, for environmental stability, these MXenes have functionalization at the outer metal atoms, further tuning their properties. It is experimentally perceived that the outer layers are often terminated with F, O, and/or OH groups, and these group's ratios and distributions strongly depend on the synthesis methods [15, 43–45].

2.2. Synthesis

For the bulk MAX phases synthesis, we recommend readers go through the literature [18, 46–50]. We focus only on its 2D counterpart. In general, MAX phases have stronger interaction in between the layers than

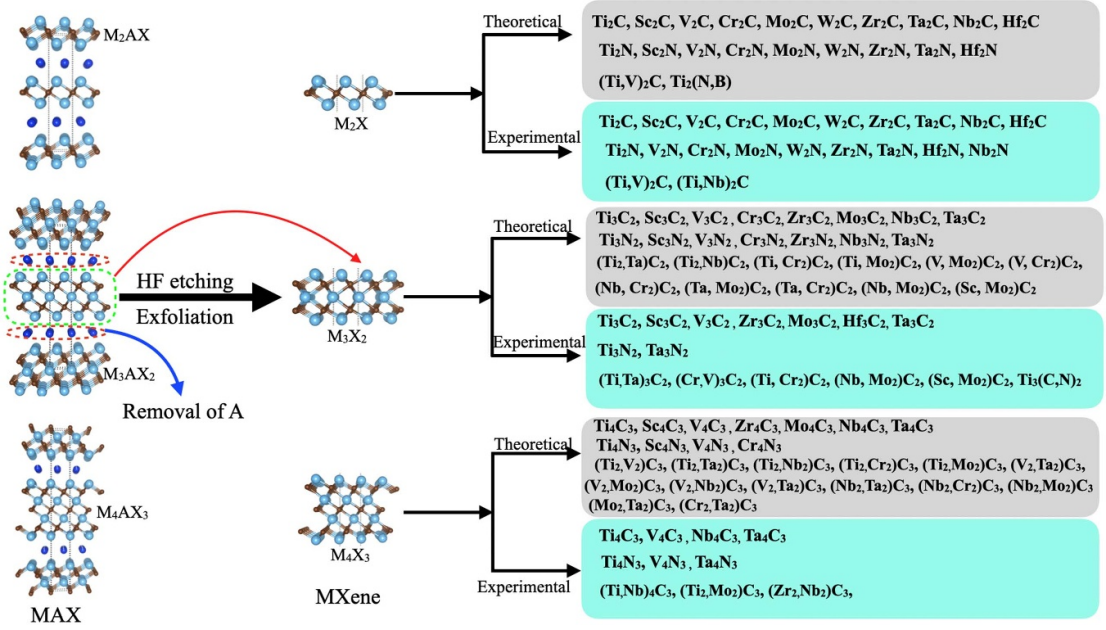

Figure 1. Crystal structure of the M_2AX (211), M_3AX_2 (312), and M_4AX_3 (413) phases in the right column, further removal of A element gives the 2D MXenes in the central column as M_2X, M_3X_2, and M_4X_3 after HF etching and exfoliation. Recent experimental and theoretical examples are tabulated in the the third column for all the three phases. Brown color balls are X(C/N), blue color balls manifests A(Al/Si) and Light blue color stand for the transition metals.

graphite, bulk black phosphorus, and MoS_2 [51–54]. The simple mechanical (scotch tape) method has difficulty in providing monolayer MXenes. The best suitable way to exfoliate monolayers and the colloidal solution of mono or few-layer is the delamination technique. Within a few years of the initial announcement in 2011, MXenes have already grown as an established class of 2DMs with exceptional possibilities in variation of chemical composition and highly tunable properties [7, 55–57]. The chemical or structural properties of MXenes are directly associated with the structural order in the bulk phases [7]. There are several steps to synthesize MXene from these bulk MAX phases, described as below:

$$Ti_3AlC_2 + 3HF \rightarrow Ti_3C_2 + AlF_3 + 3/2H_2 \quad (1)$$

$$Ti_3C_2 + 2H_2O \rightarrow Ti_3C_2(OH)_2 + H_2 \quad (2)$$

$$Ti_3C_2 + HF \rightarrow Ti_3C_2F_2 + H_2. \quad (3)$$

Due to the strong metallic M–A bond, it has not been possible to isolate the $M_{n+1}X_n$ layers and get MXenes by mechanical shearing of MAX phases. Nevertheless, M–A bonds are chemically reactive compared to the more robust M–X bonds, which makes a selective etching of A-layers possible. This selective etching is the central requirement for MXenes synthesis. In the process of MAX to MXene conversion, the etched layers are substituted by various termination groups T_z, such as hydroxyl (–OH), oxygen (–O) or fluorine (–F) [7, 18]. The material recovered after etching thus consists of $M_{n+1}X_nT_x$ multilayers attached by hydrogen and/or Van der Waals (vdW) bonds. The most used, suitable, and highly selective etchant solution for this etching is hydrofluoric acid (HF). Aluminium layers are etched by the HF from MAX phases to synthesize the MXene. The reaction occurs in this process is given in equation (1), where HF first etches the MAX phase and form the few-layer or MXene clays and AlF_3 and releases H_2. In the presence of water, one can get OH functionalized MXene, and there is also a possibility of formation of $Ti_3C_2F_2$ during the process, as described in equations (2) and (3). The details of etching conditions for a different type of beyond Al-containing MAX phase can be found in the literature [11, 18, 38, 58–64]. Overall, different MXenes can be synthesized under different etching conditions, which further gives a different quality. However, when the atomic weight of metal atoms is high, then longer time and stronger enchant solution are required due to the M–Al bonding.

HF has highly corrosive nature, it can penetrate through the skin and harm the bones and, muscle tissues. That is why an alternative to a strong HF solution should be used where possible, or one should minimize the concentration of HF. The most common alternative is the etching with a mixture of hydrochloric acid (HCl) and fluoride salt. This was first reported by Ghidiu *et al*, where they used it *in situ* experiment using lithium fluoride (LiF) and HCl on Ti_3AlC_2, and a similar result was achieved [48]. In this experiment, they concluded that the presence of proton and fluoride ions are necessary conditions for the etching process and MXene synthesis. Metal-halide presence leads to the intercalation of cations (such as Li^+) and water in MXene layers. This increases the interlayer spacing among the MXene layers and also weakens the interlayer interaction. There have been other favorable alternatives such as sodium fluoride (NaF), potassium fluoride (KF) and NH_4F with different HCl concentrations [16, 65]. Ammonium hydrogen bifluoride (NH_4HF_2) also used to synthesize thin epitaxial Ti_3AlC_2 films and powders [66]. In addition, there is an F-free etching method with an electrolyte mixture of NH_4Cl and tetra-methylammonium hydroxide (TMOAH) used on Ti_3AlC_2 with more than 40% yield [67]. Tengfei *et al* reported another promising F-free hydrothermal method was based on the Bayer process [68]. Recently, Cl-terminated $Ti_3C_2T_x$ and Ti_2CT_z MXenes have also been synthesized from of these compounds in the presence of $ZnCl_2$ Lewis acidic solution [69].

Aside from Al etching; there have been reports of Si etching from the Si based MAX phase precursors like Ti_2SiC_2 with the use of HF and hydrogen peroxide (H_2O_2) solution [70]. Nitride MXene such as $Ti_3N_2T_x$ has been also synthesized in the molten eutectic mixture of KF, LiF, and NaF at 550 °C, under argon (Ar) environment [71]. V_2NT_z and Mo_2NT_z, have been realized by the ammoniation of carbide counterpart at 600 °C [72]. Chemical etching leaves the byproduct of synthesis, such as AlF_3 salts, which has to be washed out from the yield. Hence it may need to be washed several times with water, which can functionalize the MXene with –OH [7] as it can be seen in equation (2). Acid-prewash with HCl or sulfuric acid (H_2SO_4) is also used to dissolve salts such as AlF_3 or LiF [71]. Further, the delamination process is used to exfoliate the MXene from the resultant. The suitable molecule intercalation can widen the gap in the interlayer space, weaken the interaction, and enables the exfoliation of multilayer MXene into a single layer nanosheet at a reasonably large scale [73]. For example, such as dimethyl sulfoxide (DMSO), isopropylamine, tetrabutylammonium hydroxide, chlorine hydroxide, *n*-butylamine, and urea can all be used to intercalate and followed by sonicatation to produce MXenes [74–76]. In the case of $Ti_3C_2T_x$, interlayer spacing goes from 9.8 to 17.6 Å with DMSO intercalation and in other example, Nb_2CT_z is reported to be exfoliated via the intercalation of iso-propylamine [17, 73]. Readers are suggested to go through the references for specific methods and information about the delamination process [15, 77].

2.3. Theoretically predicted MXenes

The advancement of state-of-the-art, high-throughput theoretical methods has enabled the prediction of thousands of new possibly stable materials amongst hundreds of thousand of potential combinations with the capability to effectively screen the multivariate chemical species of compounds [78–81]. The growing interest in MXenes as a new 2DMs class has fueled research to identify new phases. Due to the bottleneck in the synthesis of new 2DMs, computational efforts continue to expand, covering the prediction of materials and widening the field of their possible utilization [30]. Although computational calculations have predicted many promising 2DMs, only a few dozen of them have experimentally been realized. Still, high throughput calculations give us liberty and support for trying new kinds of materials, which further motivates experimentalists to focus their efforts to synthesize these materials. Henceforth, theoretical strategies are needed that would make it plausible to describe the electronic structure of MXenes and their heterostructures and suggest the new members of the MXene family at a fundamental level.

Various high-performance calculations have been performed on the properties and composition of MXenes lately [82]. Nathan *et al* have recently used elemental information and data from high-throughput density functional theory (DFT) computations [83] to apply the positive and unlabeled machine learning approach on 2D transition metal carbides, carbonitrides, nitrides, and their layered parent MAX phases. In their work, they identified 20 different MAX phases with a high possibility of experimental realization, which can be exfoliated to produce MXene sheets. Examples include Hf_4C_3, Ta_4N_3 and Sc_3C_2, and so on. In another work, a new form of MAX phase, Cr_2TiAlC_2 with a sandwiched Ti-layer between two outer chromium carbide layers in a M_3AX_2 structure, was calculated to be dynamically stable [40, 84]. Another study based on *ab-initio* DFT predicted and verified the stability of new, ordered, double-M MXenes phases. These have stoichiometry like $M'_2M''_2C_3$, where M' is the exterior layer metal and M'' is the internal layer metal [11]. These metals can be Ti, V, Nb, Ta, Cr, or Mo. In all these cases, carbon atoms occupy the octahedral sites between the M' and M''. Besides this, all these MXene can have several termination groups such as O, OH, or F. Several theoretical predictions of nitride Mxenes with various configurations and applications have also been reported [85–88]. Although, only a few of the nitride MXenes like V_2NT_x, $Ti_4N_3T_x$ have been experimentally synthesized till now [71, 89]. However, the theoretical discovery does not guarantee that the

corresponding MXene sheets can be synthesized, even they are energetically and thermodynamically stable in calculations. The main challenge is to find a suitable etchant. Although this gives the impression that various new MXenes would be synthesized in the future, opening the possibility of expansion of the family.

2.4. Electronic properties

The MAX phase's striking characteristics emerge from their layered structural arrangements and the mixed nature of metallic-covalent (M–X) bonds united with M–A bonds that are comparatively weak compared to the former one [18, 35, 46, 47, 90]. These exceptional combinations make MAX phases suitable for a broad range of applications, varying from sensors, electrical contacts, microelectromechanical systems, protective coatings, and many more [28, 39, 91]. The electronic structures of the first few MXene phases were established rapidly [92–94]. Similar to MAX phases, most of the pristine MXenes have a metallic electronic structure. In DFT calculations, Ti_3C_2 was found to be metallic, but further the functionalization of this MXene can effectively change the electronic structure from metal to semiconductor [7, 13]. The electrical conductance of $Ti_3C_2T_x$ has attained 3250 S m^{-1}, which is eventually higher than that of graphene (2500 S m^{-1}) [52, 95]. An extensive DFT investigation was performed by Kazari *et al* for various metal nitride M_2N (M = Sc, Ti, C, Cr, Zr, Nb, Ta) and metal carbide M_2N (M = Cr, Ti, Zr) with the saturation of metal atoms with O, OH, and F [41, 96]. Theoretically, it has been suggested that both F and OH groups affect the electronic structure of MXenes in the same order because they withdraw only one electron from the surface. On the other hand, O termination is different and has the capability of withdrawing two electrons from the surface to be stabilized [10]. Sulfur (S) terminated nitride MXenes also reported for metallic behavior and good electrochechmical properties [86]. Most of the functionalized MXenes were found to be metallic and magnetic with some exceptions. Only a handful of them, such as Sc_2CT_2 (T = O, F, OH), Cr_2CT_2 (T = OH, F), and Ti_2CO_2 are semiconductors, whereas Cr_2NT_2 (T = O, F, OH) and Cr_2CT_2 (T = F, OH) are magnetic [97, 98]. However, all these MXenes mentioned above have indirect bandgap, excluding $Sc_2C(OH)_2$, which has a small direct bandgap [10]. Lee *et al* studied the strain effect on Sc_2CO_2, which suggest that with the increase in tensile strain, the bandgap gradually decreases [99]. At a critical tensile strain, the indirect bandgap changes to a direct one. External electric field can also tune the gap from indirect-to-direct bandgap [100, 101]. The electronic properties have been experimentally verified for selected MXene such as Ti_2C, Ti_3C_2, Mo_2C [102–105].

Furthermore, the multiple-metal-atom MXenes open the possibilities for a range of potential applications, owing to their lower symmetry and the capability to choose combinations of metal atoms, which tailors the chemical and electronic properties. Dong *et al* predicted possible spintronic materials with robust ferromagnetism in $Ti_2MnC_2T_x$ independent of surface functionalization, similar in oxidized $Hf_2MnC_2O_2$ and $Hf_2VC_2O_2$ [106]. Lately, Sun *et al* investigated a series of surface-metal and termination-dependent metal–insulator transitions in $TiCr_2N_2$ and $TiMn_2N_2$ with Ti as the middle layer [107]. $Mo_2TiC_2T_x$, $Mo_2Ti_2C_3T_x$, and $Cr_2TiC_2T_x$ were experimentally realized and manifested to have distinct electrochemical properties from that of the conventional single-metal Ti–C based MXenes [11, 108]. Besides these, Tao *et al* designed a new i-MAX phase in 2017 with stoichiometry $(Mo_{2/3}Sc_{1/2})_2AlC$, with in-plane chemical ordering of the Sc and Mo atoms [62]. Selective etching made it possible to remove both the Al and Sc atoms and resulted in 2D MXene $Mo_{4/3}C$ sheets. The initially characterized capacitance showed the value of 1153 F cm^{-3} and 339 F g^{-1}, which exceeds those of Mo_2C by 65% and 28%, respectively. Khazaei *et al* predicted that certain combinations of i-MXene may display semiconducting nature, due to the lack of centrosymmetric, and can exhibit piezoelectric properties [109]. i-MXenes can be advantageous for properties that are profoundly surface geometry dependent. We also encourage readers to go through the literature for mechanical properties of the MXenes [43, 71, 98, 110, 111].

3. 2D MXene based electrodes for rechargeable batteries

High performance demands on electrochemical energy storage systems have become increasingly important. Unquestionably, the efficiency of rechargeable battery electrodes depends largely on the successful design and implementation of electrode materials. The specifications for potential energy storage materials consist of: (a) good reversible redox-reaction; (b) easy access to electrolyte ions; (c) sufficient number of adsorption sites; (d) high electrical conductivity. Over the last few years, a large number of 2DMs have demonstrated considerable benefits in the area of electrochemical energy storage owing to both their large surface area as well as their relatively fast ion transport pathway. With only a single or few atomic layers thickness, multiple surface active sites and excellent mechanical characteristics, 2DMs fulfill the challenges of electrochemical energy storage technologies, especially rechargeable batteries. As mentioned in the previous section, roughly 20 different types of MXene have been successfully synthesized and many important breakthroughs have been achieved in the energy storage area, owing to their outstanding and distinctive structure,

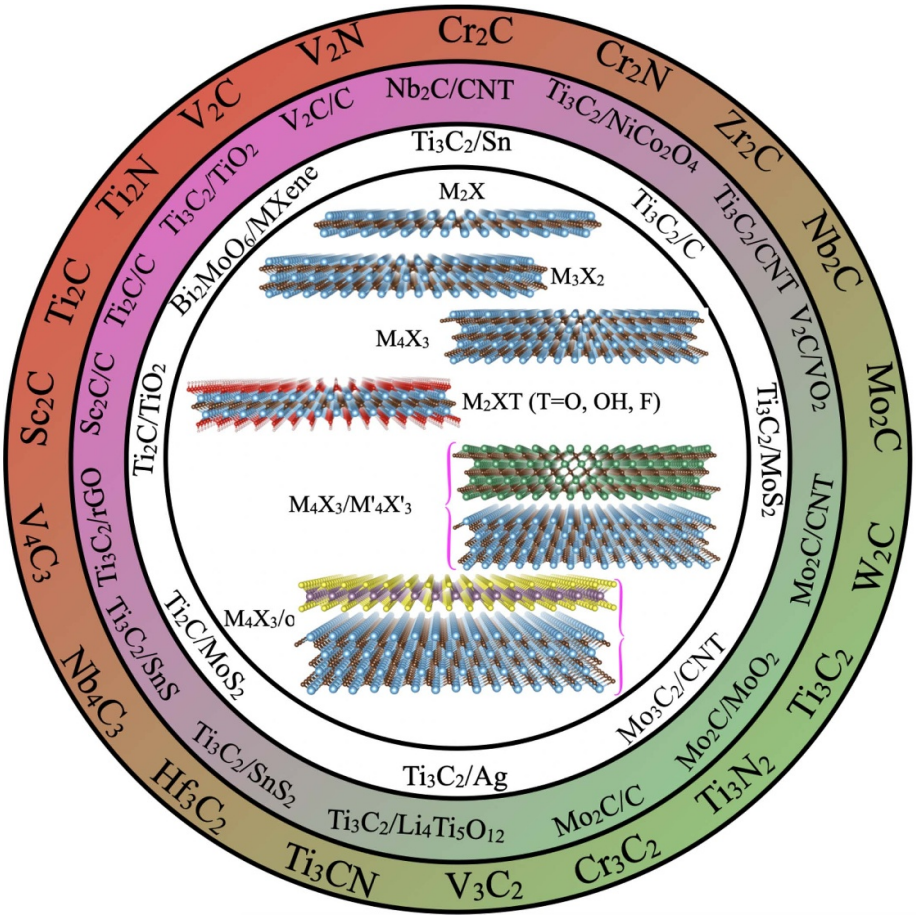

Figure 2. Schematic illustration of current MXene materials investigated in Energy Storage applications. The structures of MXenes have three different formulas such as M_2X, M_3X_2 and M_4X_3 in which M represents the transition metal and X is carbon (C)/nitrogen(N). The rechargeable battery has been done on the different form for example, Ti_2C, Nb_4C_3) and their hybrid heterostructures.

high-conductivity, high ionic-diffusion and other advantages compared to other 2DMs. Based on the 2D features as well as superior electrical conductivity of MXene materials, they represent an alternative for high-performance electrochemical rechargeable batteries including metal-ions and Li–sulfur batteries. In this context, it is of utmost necessity to survey and summarize the most recent progress of MXenes as promising battery electrodes.

3.1. 2D MXene for alkali metal-ion batteries

In recent years, a large amount of computational and experimental researches have been carried out in order to design new materials for negative electrodes in Li-ion and non-Li-ion batteries, with high storage capacity, high safety performance and low volume expansion (summarized lists of MXenes materials in figure 2). Among the family of 2DMs which have attracted a lot of interest 2D $M_{n+1}X_nT_x$ MXenes (with $n = 1$–3, M: transition-metal, X: Carbon and/or Nitrogen-atom and T: hydroxyl, oxygen or fluorine) has been reported to be the upcoming promising alternatives for graphite 2DMs as anodes (see figure 2), owing to their unique properties including great carrying capacity, a huge surface area with more space for the intercalation of alkali metal ions, as well as the surface activity derived from the transition-metal surface terminated by OH-, O- or F-groups [18, 19, 23, 23, 112]. In this section, we will highlight some recent breakthroughs achieved in metal-ion batteries by focusing on the electrochemical efficiency of MXenes as a negative electrode.

Interesting progress has been achieved through the experimental process. It was established on the basis of gravimetric capacity that bare 2D $M_{n+1}X_n$ MXenes with $n = 2$ are more promising and can store a high number amount of metal-ions per gram compared to bare M_3X_2 and M_4X_3 layers. Naguib's group have studied the possibility of using Ti_2C and Ti_3C_2 layers as anode for Li-ion batteries and concluded Ti_2C exhibits a gravimetric capacity about 50% higher than that of Ti_3C_2 [73, 113]. It was further determined in the case of Ti_2C that lithiation/delithiation peaks are located at 1.6–2.0 V relative to Li^+/Li with a gravimetric capacity of 225 $mAhg^{-1}$ [113] and that the gravimetric capacity of Ti_2CT_x is about 1.5 times greater than that of $Ti_3C_2T_x$ [73]. Subsequently, niobium and vanadium carbides, namely Nb_2C and V_2C, have been

tested as electrode materials for Li-ion batteries showing ability to handle high charge/discharge rates with reversible capacities of about 170–260 $mAhg^{-1}$ at 1 C in the case of the Nb_2C layer, and 100–125 $mAhg^{-1}$ at 10 C in the case of the V_2C layer [9]. Tang *et al* have reported the feasibility to use Ti_3C_2 monolayer with its F- and OH-functionalized surfaces as a promising active materials for Li-ion batteries. Adopting DFT they have found that Ti_3C_2 sheet has outstanding electrochemical characteristics when used as anode for Li-ion batteries, such as significant adsorption energies of about −0.504 eV/Li-atom, low diffusion barrier of 0.07 eV, low profile insertion of 0.62 V *vs.* Li/Li^+ and corresponding theoretical specific capacity of 320 $mAhg^{-1}$ compared to $Ti_3C_2F_2$ (130 $mAhg^{-1}$) and $Ti_3C_2(OH)_2$ (67 $mAhg^{-1}$). Xie *et al* systematically explored using theoretical calculations combined with experiments, the interaction between Li-ion and different functionalized 2D transition-metal carbides including Sc_2C, Ti_2C, Ti_3C_2, V_2C, Cr_2C, and Nb_2C [18, 114]. They have found that the capacity of Li-ion storage is mainly dependent on the type of surface functional groups and that the O-terminated MXenes exhibit the highest specific capacities (see table 5). Additionally the computed Li-diffusion barriers confirm great Li-mobilities [18, 114] with the possibility that Li-atoms can form an additional layer due to the high electrical conductivity of MXenes.

MXenes also demonstrated encouraging performance in terms of specific capacity and stability for non-lithium ion batteries. Table 4 summarizes the capacity and stability in non-lithium ion battery applications of $Ti_3C_2T_x$ [19, 115–119]. Xie *et al* have investigated a family of 2D transition metal carbides for promising anodes in non-Li ion batteries including Na, K, Mg, Ca, etc by using both DFT and experiments [120]. They have found that the O-functionalized surface and bare MXenes present a great theoretical specific capacity and proved to be promising anode materials for non-li ion batteries. Furthermore, Vivek *et al* have modeled recently the S-functionalized nitride MXenes, namely Ti_2NS_2 and V_2NS_2 and their possibility to use as active materials in Li- and Na-ion batteries by using first principle modeling [86]. Based on the fact these materials exhibit a high conductivity, the Li-ion can form reversible multi-layer ion intercalation, which manifest high theoretical specific capacity (see table 5).

Zinc hybrid-ion batteries are also a suitable substitute to expensive Li-ion batteries. In these batteries, Zn-metal works as an negative electrode and exhibit outstanding features among the many mentioned electrochemical batteries owing to their high theoretical specific capacity of 820 mAh g^{-1}, and low diffusion profile of about 0.76 V compared to the standard electrode. Significant breakthroughs have been achieved toward this type of rechargeable batteries for cathode materials, such as manganese and vanadium oxide. Although a high-capacity has been achieved in these cathode materials but unfortunately they show lower potential voltage of less than 1.0 V. In order to overcome these challenges, Xinliang *et al* [121] have recently fabricated a zinc hybrid-ion battery cathode through a phase transition process, which can significantly enhances battery capacity, resulting in adequate capacity and cycling stability. They have demonstrated the higher potential of the V_2CT_x for zinc hybrid-ion battery, and provide an efficient approach to attain enhanced battery efficiency through the introduction of a phase transition appropriate to the electrode materials (see figure 3). This demonstrates that the Li^+/Zn^{2+} insertion leads to the improvement of layer spacing of the V_2CT_x, which facilitates the further insertion and extraction of ions.To summarize, from the brief collection of the latest experimental results, it is clear that MXenes and functionalized of MXenes offer a promising performance when used as anode in Li and non-Li ion batteries. Theoretical considerations based on DFT are expected to provide guidance for the selection as well as the optimization of potential MXene-based anodes.

3.2. 2D MXenes as host materials for lithium–sulfur batteries

Recently, lithium–sulfur (Li–S) batteries have attracted widespread interest as a promising and upcoming non-toxic and eco-friendly alternative in electrochemical storage systems. Li–S batteries show significantly higher theoretical specific capacity (about 1675 $mAhg^{-1}$ for S-containing cathode and 3860 $mAhg^{-1}$ for metallic Li-anode) and energy density (2500 $Whkg^{-1}$ taking into account full reaction to Li_2S) over those of conventional alkali metal-ion batteries [126–128]. These batteries mainly consist of a Li-metal anodes, an S-containing cathodes and a separator which is impregnated with organic electrolyte [129, 130]. Figures 4(a) and 6 depicts a schematic illustration of a standard Li–S battery, based on the conversion process: $16Li + S_8 \rightleftharpoons 8Li_2S$. During the discharge process, the Li-anode releases Li^+-ions and electrons (e^-), Subsequently, these Li^+-ions diffuse to the positive electrode via liquid electrolyte [131]. Simultaneously, the e^- switch over from external-circuit to sulfur-cathode, and S_8 gets reduced to long chain lithium poly-sulfides (Li_2S_n with $n \geq 4$) according to the following reactions [132]: $2Li^+ + S_8 + 2e^- \mapsto Li_2S_8$, $3Li_2S_8 + 2Li^+ + 2e^- \mapsto 4Li_2S_6$, $Li_2S_8 + 2Li^+ + 2e^- \mapsto 2Li_2S_4$. Further Li_2S_4 reacts with Li to form short-chain Li_2S_n ($n = 2,1$) in following reactions: $Li_2S_4 + 2Li^+ + 2e^- \mapsto 2Li_2S_2$, $Li_2S_2 + 2Li^+ + 2e^- \mapsto 2Li_2S$.

Despite above-mentioned advantages and the flexibility of Li–S batteries, their practical implementation in day-to-day life remains challenging due to many crucial issues related to the sulfur cathode, e.g. the shuttling effect of intermediate soluble Li_2S_n with $3 \leq n \leq 8$), high volume change of sulfur and electrical

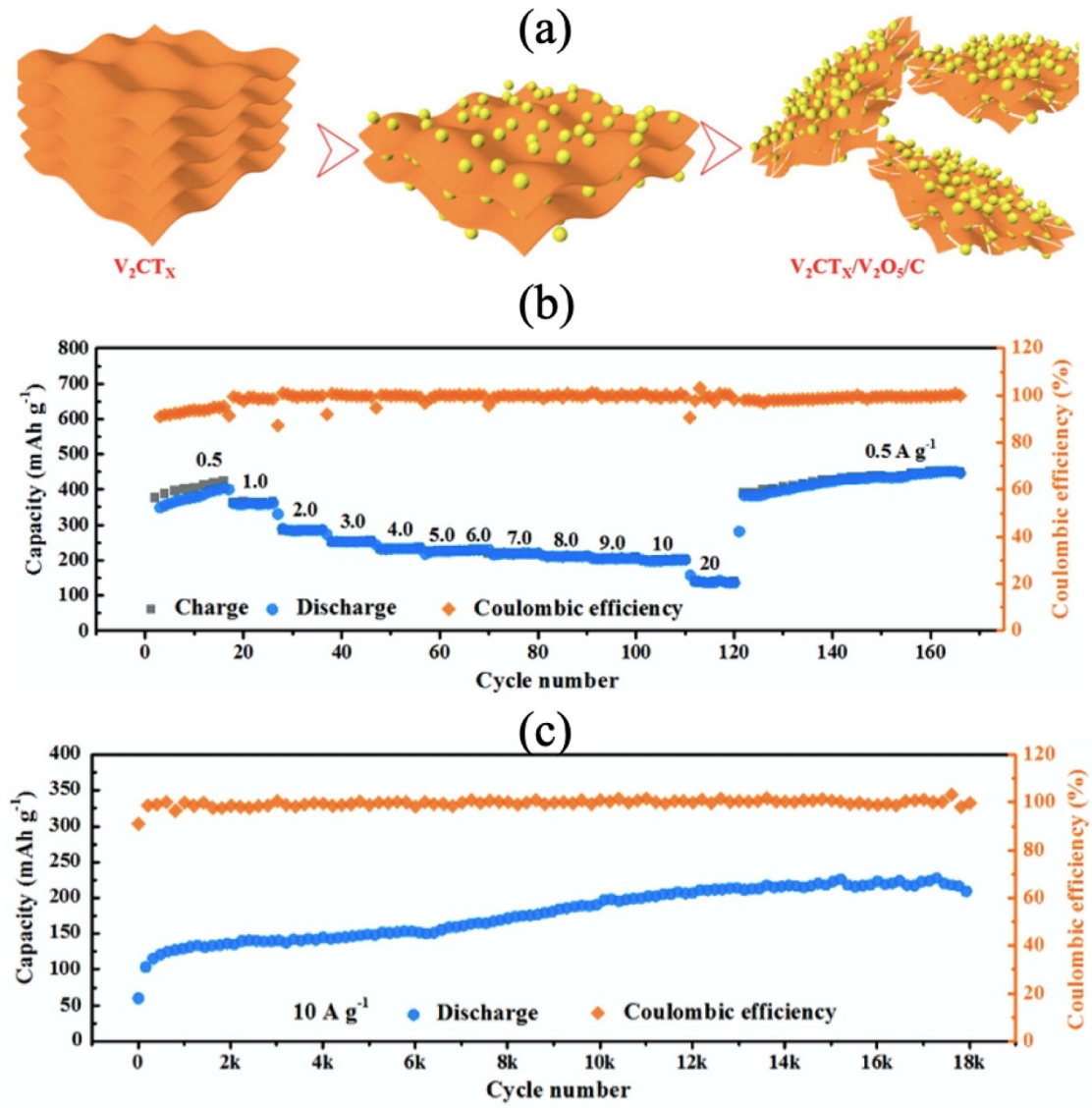

Figure 3. (a) Schematic representation of the possible mechanism of the structural and phase transition of the V_2CT_x MXene cathode, (b) rate performance at different current densities and (c) a very long cycling performance at the current density of 10 Ag-1 after 18 000 cycles of the V_2CT_x MXene structure for the zinc hybrid ion storage performance. Reproduced from [121]. Copyright 2020, American Chemical Society.

insulating nature of S and the short-chain polysulfides (Li_2S_2 and Li_2S) as illustrated in figure 4(b). A description of these critical issues are discussed briefly in the following sections:

1. **Shuttle effect**: This corresponds to the diffusion back-and-forth of Li_2S_n polysulfides between the Li-metal anode and S-containing cathode. In other words, it is produced through the dissolution of Li_2S_n in the liquid electrolyte (see figure 4(a)). During discharging and charging process, once the solid sulfur in S-containing cathode is reduced to long-chain Li_2S_n ($n = 8,6,4$) polysulfides, which dissolve into the liquid-electrolyte and react with the Li-metal anode. In the process, they are electro-chemically transformed into short-chain Li_2S and Li_2S_2 polysulfides, resulting the loss of the active materials. Subsequently, Li_2S and Li_2S_2 re-diffuse to the S-containing cathode and form long-chain polysulfides during charging process, followed by re-diffusion of long-chain polysulfides again towards the anode side, provoking an irreversible loss of sulfur, insufficient Coulombic performance, auto-discharge processes and poor cycle stability [133].
2. **Large volume expansion of S**: Considerably higher crystalline density of sulfur (approximately 2.07 g cm^{-3}) compared to that of lithium polysulfides leads to a significant volume expansion of about ~ 80% during the lithiation process. The successive volume expansion/contraction throughout the discharging/charging cycles causes fragmentation of the active materials, leading to considerable structural instability of the electrode, quick capacity decay and safety issues [134].

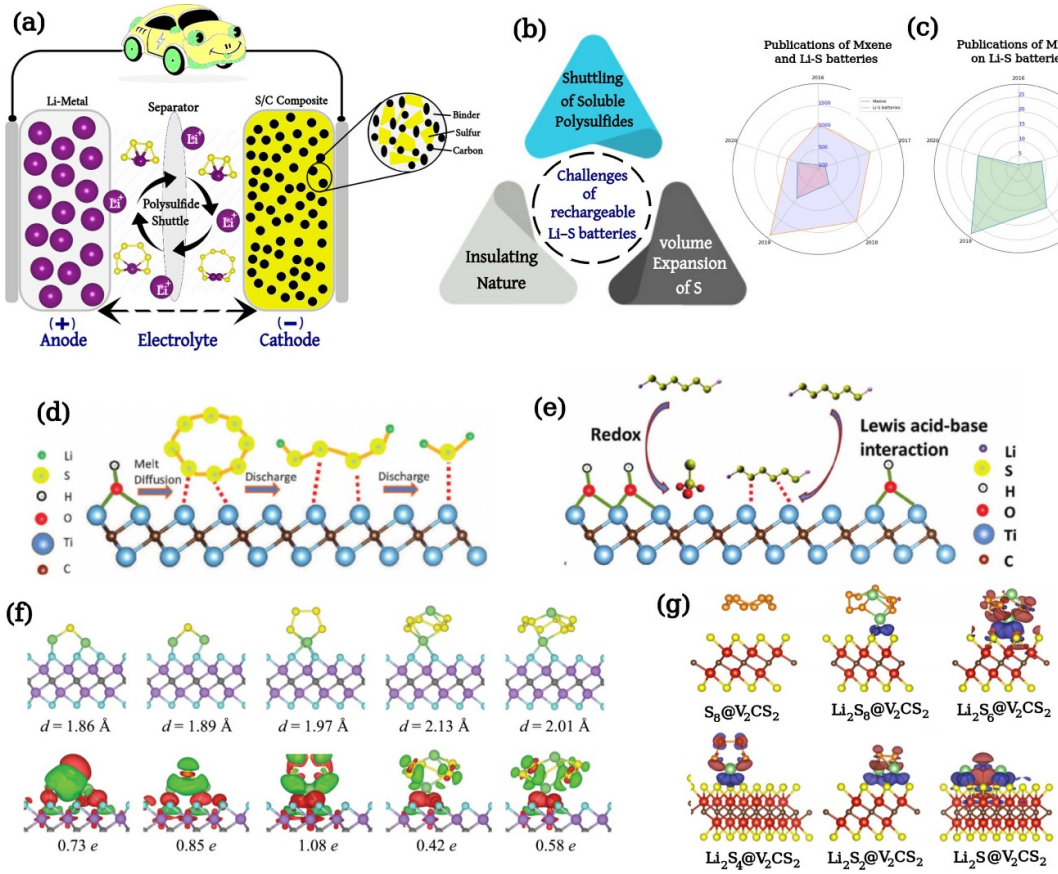

Figure 4. (a) A schematic illustration of the operation principle of Li–S batteries, which consists mainly of a Li-metal anode, a sulfur/Carbon cathode, a separator, and the electrolyte; (b) Overview of challenges in the development of advanced Li–S batteries; (c) The number of publications per years on MXene, Li–S batteries and MXene-based Li–S batteries from Mendeley; (d) A schematic of the interaction between MXene phase and Li_2S_n via Ti–S bond. Reproduced with permission from [122]. Copyright 2015 by the Wiley Online Library; (e) the interaction between OH-decorated 2D MXene and Li_2S_n species depicted in a two-step process. Reproduced with permission from [123]. Copyright 2016 by John Wiley and Sons; (f) the most stable configurations of Li_2S_n adsorbed on Ti_2CF_2 and the Charge transfers between LiPSs and Ti_2CF_2. Red and green represent the spatial regions gain (loss) in charge. Reproduced from [124] with unrestricted use permission;(g) difference Charge density of LiPSs adsorbed on V_2CS_2. Red and blue zone represent charge accumulation and depletion, respectively. Reproduced with permission [125]. Copyright 2019 by Royal Society of Chemistry.

3. **Insulating nature of S, Li_2S and Li_2S_2**: While Li–S batteries are in operation, Li_2S and Li_2S_2 are susceptible to coating the sulfur and hindering its further utilization. Therefore, a significant quantity of conductive carbon additive is required to ensure both the electron transport and the electrochemical reaction which results poor gravimetric-capacity [135].

Significant progress has been undertaken toward designing of modern and innovative cathode materials to overcome all the aforementioned limitations, in particular 'Shuttle effect of soluble LiPSs' [136]. A typical advancement during early investigations was the implementation of porous conductive carbon as cathode of Li–S batteries [137–139]. Nevertheless, the introduction of porous carbon based cathode materials and LiPSs are not sufficient to hinder the migration and diffusion of soluble LiPSs. This leads to low cycling-stability over the long term charge/discharge process. It has been recently revealed by studying a wide category of materials, based on graphene oxides [140, 141], metal-oxides such as TiO_2 and MnO_2 [142, 143], and metal–organic frameworks (MOFs) [144, 145]. The crucial and important factor to overcome is the LiPSs migration and to achieve a long cell life, which consists strong chemical interactions over time between the host materials and the dissolved LiPSs. However, several of these materials do not possess the characteristics required for effective cathode, namely good mechanical stability and excellent electronic conductivity. In this context, MXenes can potentially fulfill a crucial role owing to their capability of achieving high-electronic conductivity as well as a significant surface area characteristics, which can enhance the electron diffusion between electrodes and improve the chemical interaction of the sulfur cathode with LiPSs. This has led to widespread interest with a growing number of publications in recent years as shown in figure 4(c).

DFT based first principles calculations have yielded a relevant criteria for the theoretical strength of LiPSs/MXene interaction based on binding energies, which is the difference between the total energies of the

Table 1. Summary of binding/adsorption energies for Li_2S_n (with $n = 1,2,4,6,8$) and S_8 species on 2D MXenes and functionalized-based 2D MXenes.

Host Materials	Li_2S	Li_2S_2	Li_2S_4	Li_2S_6	Li_2S_8	S_8	Reference
Ti_2C	5.82	8.87	15.41	22.71	29.73	–	[150]
Ti_3C_2	5.68	8.78	15.21	21.96	29.54	–	[150]
Ti_2N	6.09	9.16	15.85	22.47	29.18	–	[150]
Ti_3N_2	6.13	9.21	15.59	22.62	29.33	–	[150]
V_2C	6.42	9.61	12.19	19.69	15.27	19.52	[125]
$V_2C(O)_2$	4.42	3.80	2.91	2.48	3.06	1.07	[125]
$V_2C(S)_2$	2.16	1.89	1.31	1.05	1.10	0.69	[125]
$Ti_2C(OH)_2$	–	–	3.43	4.49	4.90	–	[150]
Ti_2CO_2	–	–	2.58	1.53	1.72	–	[124]
	3.02	3.12	1.92	1.47	1.71	0.95	[146]
TiS_2	–	–	1.59	1.51	1.30	–	[124]
Ti_2CF_2	2.36	2.14	1.61	1.28	4.51	–	[124]
	–	–	1.02	0.42	0.34	–	[146]
	–	–	1.11	1.03	1.15	–	[148]
$Ti_3C_2F_2$	–	–	1.95	1.54	1.69	–	[124]
	–	–	0.85	0.43	1.15	–	[146]
$Ti_3C_2O_2$	–	–	1.44	2.05	1.78	–	[146]

optimized MXene+LiPSs system and summation of MXenes system without LiPSs and isolated LiPSs. Zhao *et al* have demonstrated a promising host material for trapping soluble S-containing polysulfides in oxygen functionalized titanium carbide-based MXenes, namely Ti_2CO_2 and $Ti_3C_2O_2$, which comes from the attraction between the positively charged Li-ions in Li_2S_n polysuflides and negatively charged oxygen-atoms. This leads to relatively high binding energies ranging from 1 to 2 eV (see table 1) [146]. Chung *et al* have investigated the impact of different non-uniform surface including the substitutions, vacancy, and S-trapped sites of fluorine and oxygen functionalized Ti_2C for anchoring characteristics of S-containing species (Li_2S_n) [147, 148]. Through an energetic analysis, they have confirmed that Ti_2CF_2 successfully suppresses the shuttling of LiPSs, while the neutralization of soluble long-chain polysulfides to insoluble elemental sulfur on Ti_2CO_2 eliminates the shuttling.

Liang *et al* reported Ti_2CT_x as a sulfur host materials of the cathode, which enhances the performance of Li–S batteries [122, 123]. It has been noticed on the basis of the ion-electron pairs nature of S-atoms [149] that the polysulfides are able to act as soft bases, which means that the MXene host without terminal groups may strongly interact with the polysulphides via the Ti-S coordination (see figure 4(d)) [122]. Furthermore, recent findings by Nazar's group provide insights into the formation of Ti–S bonds with the formation of a great quantity of thiosulfate-polythionate molecules on the surfaces of host-materials upon the contact with polysuflides [143]. Figure 4(e) illustrates the interaction between OH-decorated MXene and Li_2S_n species which can be described in a two-step process [123]: I) the Li_2S_n species are initially chemisorbed on the MXene surface, undergo redox reactions with the OH-terminations and form thiosulphate groups, II) the titanium atoms easily accept extra Li_2S_n polysulfides in the electrolyte which forms Ti-S bonds through acid-Lewis base interactions.

Min Fang *et al* described the effect of many-body dispersion (MBD) in on the binding energies of polysulfides on Ti_2CF_2 as host materials, and further discussed the anchoring mechanism of Li_2S_n polysulfide reduction [124]. They found by comparing the Li_2S_n polysulfides, that Li_2S_4 tends to adsorb vertically on Ti_2CF_2 with the both Li-atoms binding with Ti_2CF_2 due to strong Li–F interaction (see figure 4(f)). MBD method predicts the lower binding energies over 20% compared to vdW^{surf} method in the case of long chain polysulfides with the ratio for many-body effect range between 16.8% and 33.3% during the delithiation of Li_2S_n polysulfides. Based on experimental approach, Tang *et al* also reported that $Ti_3C_2T_x$ with nanoscale S uniformly decorated on the surface have the enhanced performance of very $Ti_3C_2T_x$ (see table 2) [151, 152]. A recent computational study by Wang *et al* investigated the feasibility of S functionalization of MXenes to create a sulfur rich cathode. This showed that vanadium carbide with S-functionalization (V_2CS_2) presents a enhanced binding energy (see table 1 and figure 4(g)). This suppresses the shuttling of soluble polysulfides by preventing the decomposition of the Li_2S_n polysulfides [125]. Unlike the standard conductive hosts for S-cathodes, MXenes have the potential to effectively trap Li_2S_n LiPSs during the discharge/charge for Li–S batteries. MXenes with functionalization can additionally enhance the binding capacity of Li_2S_n polysulfides, which suppress the shuttle effect of soluble polysulfides in Li–S batteries.

Table 2. Electrochemical characteristics summary of experimental advances MXene as cathode hosts for Li–S battery, e.g, current rate (C), cycle number, reversible capacity ($mAhg^{-1}$) and electrochemical mechanism.

Hosts materials	Rate (C)	Cycle number	RC ($mAhg^{-1}$)	Electrochemical mechanism	Reference
S@$Ti_3C_2T_x$	0.2	800	724	Double mechanism	[151]
Ti_2C-S	0.5	400	960	Chemical adsorption	[150]
$Ti_3C_2T_x$/S	1	1000	689.7	Chemical adsorption	[153]
$Li_2S/Ti_3C_2T_x$	0.1	100	525	Chemical adsorption	[154]
$Ti_3C_2T_x$/rGO/S	1	500	596	Chemical adsorption	[155]
$Ti_3C_2T_x$ /(1 T-2 H)-MoS_2-C-S	0.5	300	799.3	Electrocatalysis	[152]
S@TiO_2/Ti_2C	2	200	464	Chemical adsorption	[156]
$Ti_3C_2T_x$/CNT	0.5	1200	1240	Double mechanism	[123]
$Ti_3C_2T_x$/graphene/Li_2S	0.2	100	710	Dual chemisorption	[157]
$Ti_3C_2T_x/MnO_2$	0.2	500	1140	Electrostatic self-assembly	[158]
Mo_2C/C	1	600	1050	Chemical adsorption	[159]
Mo_2C/CNFs	0.1	50	1017	physical/chemical adsorption	[160]
W_2C NPs/CNFs	1	500	1200	Dual chemisorption	[161]
W_2C/N/P-rGO	1	400	914	Chemical adsorption	[162]

4. Van der waals heteroctruture for energy storage

4.1. Types of heterostructures

The standard method to improve the performances of electrochemical properties of 2D layered materials, including MXenes, is by hybridization with complementary materials into multifunctional heterostructures or composites, including 0D–2D, 1D–2D, 2D–2D, and lateral-2D structures constructed from low-dimensional ingredient nanostructures. In this section, we will review the emerging applications of 2D heterostructures that enhances the performance in the field of electrochemical storage. The numerous nanostructures with different dimensionalities, such as quantum dots (QDs)/nanoparticles (0D), nanotube/nanorods (1D), and 2D nanosheets, have been established to hybridize with 2D MXene nanosheets to form heterostructures as presented in figure 5. These hybridizations can substantially improve the overall electronic conductivity, especially for the heterostructures hybridized with a conductive matrix, such as carbon-nanotubes (CNTs), different nanoparticles, and conductive polymers, etc [77]. The expansion of volume during the insertion process can also be effectively tuned by the designed porous and hollow hybrid structures and it shows better performance for electrochemical energy storage including lithium ions battery (LIB) and other batteries [54, 77, 163–167].

Two main categories of heterostructures corresponding to the wide range of applications are vertically stacked heterostructure (see in figure 5(c)) and horizontal in-plane (lateral) heterostructure (see in figure 5(d)). The vertically stacked heterostructures are those in which two or more 2DMs have interfacial contact, and it may be either due to strong (i.e. covalent) or weak (i.e. vdW) interactions. The sequence of stacking is significant because it may change the physical and chemical properties, modulated by different stacking orders. Also, the horizontal or lateral heterointerfaces have at least two different 2DMs joined together at the edge results in strong bonding between the edge atoms. The 2D hybrid heterostructures have demonstrated their competency by outperforming potential devices made from mono-layered 2DMs. This improvement is attributed to synergistic effects caused by close interaction between different materials, which may result in considerable changes in physical and chemical properties that ultimately allow us to modulate or activate useful features for various applications.

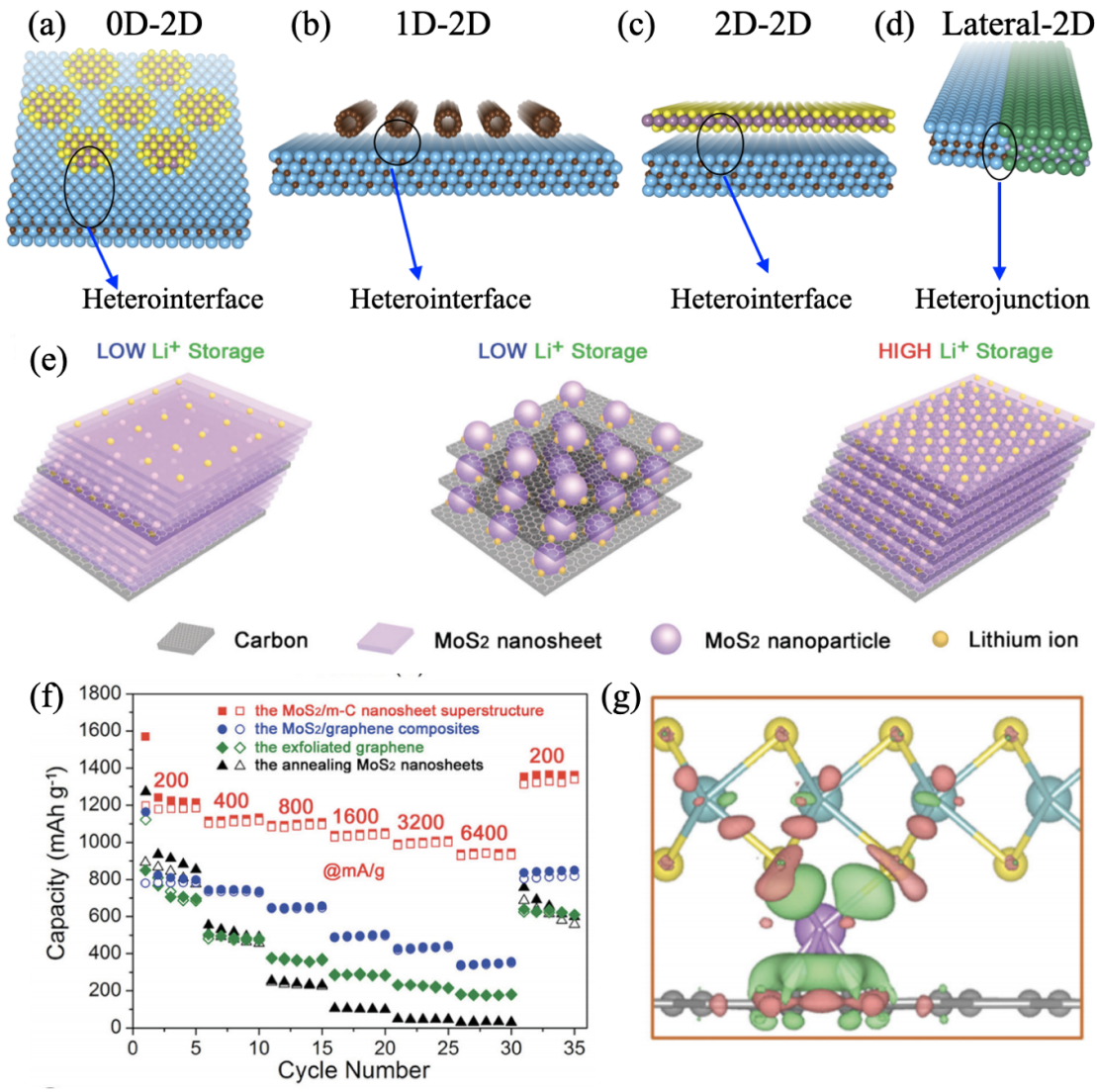

Figure 5. Schematic representation of 2D heterostructures (a) vertical heterostructure with quantum-dot (0D) and single 2D heterointerface and (b) vertical heterostructure with one-dimensional (1D) nanotube and 2D heterostructure), (c) vertical heterostructure with 2D heterointerface, and (d) horizontal in-plane heterostructure (with 2D heterojunction). The black circle represents the heterointerface/heterojunction in the hybrid 2D heterostructures. (e) The concept of the rational design of the MoS_2/m-C nanosheet superstructure for constructing ideal MoS_2/C atomic interfaces to enhance lithium-ion storage, (f) the capacity retention of the MoS_2/m-C nanosheet superstructure, MoS_2/graphene composites, exfoliated graphene, and the annealed MoS_2 nanosheets at current densities from 200 to 6400 mAg^{-1} and (g) 3D charge density difference plot in Li adsorption at the MoS_2/G interface, in which green and dark red color indicates the electron accumulation and depletion [168]. Reproduced from [168]. Copyright 2015, Wiley-VCH.

2D heterostructures are generally synthesized by using a single 2D nanomaterial as a substrate, then adding secondary layers via either in a 'top-down' or 'bottom-up' approach. The solid-based techniques [169–171] have shown special importance for energy storage and conversion. Large, high quality nanosheets cannot be made via chemical vapor deposition (CVD) [172, 173], however the technique can synthesize relatively small nanosheets for 2D heterostructures for energy storage and conversion. The energy-related applications are sensitive to surface [174], porosity [175] and electrolyte exposed active edge sites [19, 54, 176–180]. The 2D hybrid heterostructures can help to overcome the limitations of single 2DMs, distinct from the various supercapacitor and the battery performance improvements achieved recently. The Ragone plot (i.e. energy density vs. power density) of batteries offer low power density and high energy density, whereas supercapacitors have vice-versa. Jiang *et al* [168] synthesized a novel 2D hybrid nanosheet superstructure consisting of the alternative atomic interface contact/interaction between single-layer MoS_2 and single-layer carbon nanosheet with very limited interface contact as shown in figure 5(e). It was reported that the optimized MoS_2/m-C hybrid superstructure solves most of the key challenges for MoS_2-base anode materials for LIBs, such as poor electrical conductivity of MoS_2 along the perpendicular direction, accommodating the volume expansion upon lithiation, overcoming the aggregation and restacking of MoS_2

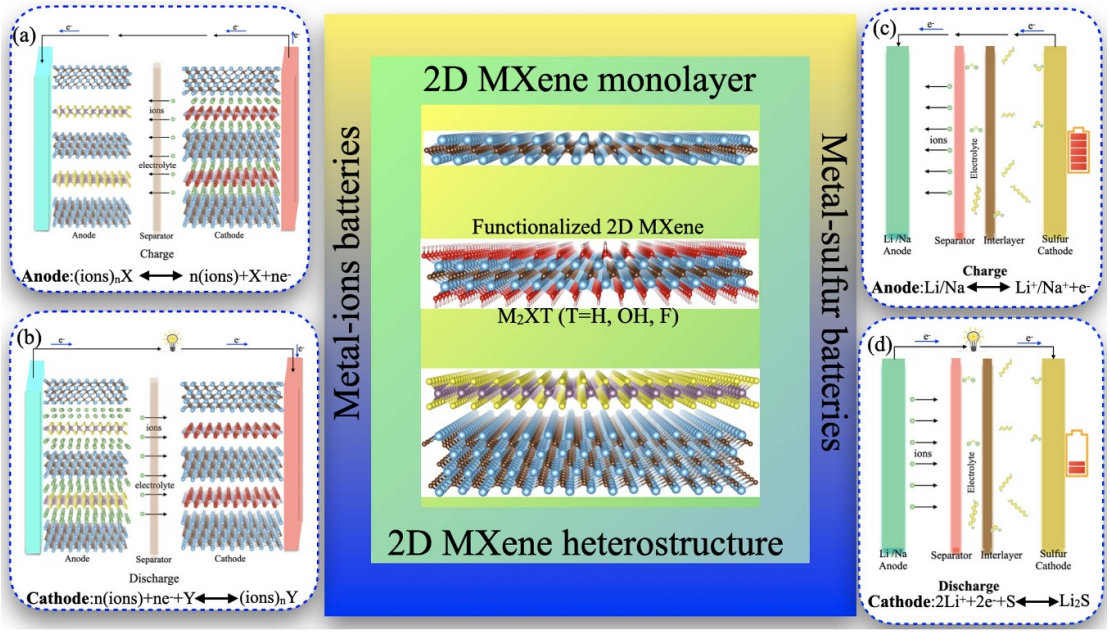

Figure 6. Overview of 2D MXene hybrid materials for batteries. (a), (b) Schematic illustration of the configuration of anode/cathode for rechargeable metal-ion batteries (X/Y represents the anode/cathode material, respectively). (c), (d) Schematic illustration of a hybrid anode/cathode of lithium–sulfur batteries.

layered material, providing the largest interface contact for Li-ion storage and also for mitigating the polysulfide shutting [168]. A MoS_2/m-C nanosheet superstructure has been demonstrated as an anode materials for Li-ion storage in which it exhibits a high reversible specific capacity of 1183 $mAhg^{-1}$ at current density of 200 mAg^{-1}, shown in figure 5(f). From the DFT investigations, the MoS_2/m-C hybrid superstructure interface provided the most energetically favored process for high Li-ion storage and demonstrating the explicit synergetic effect between MoS_2 and single-layer of carbon nanosheet as shown in figure 5(g). Besides this, other MoS_2-based hybrid superstructures displayed good battery performances [181–184]. In the next section, we will discuss some recent advances about 2D hybrid heterostructures for batteries to recount their promising potential in this field.

4.2. Lithium ions batteries

Generally, conventional LIBs use graphite as the anode. The limitations of graphite such as low specific capacity 372 $mAhg^{-1}$ and poor rate capability motivate researchers to focus on the new smart 2DMs such as graphene and other monoelemental, TMDs, MXenes etc. The single layer of graphene appeared to have a moderate capacity, unavailable voltage platform, and low Coulombic efficiency. The single layer of MXene also shows relatively low specific capacity as compared to their hybrid heterostructures [19, 21, 23]. As discussed in earlier sections, most of the MXenes are potential candidates who have displayed high electrical conductivity, fast molecular and ion transport, low operating voltages, and high storage capacities [19, 185]. The cyclic voltammogram measurements of single layer of Ti_3C_2 nanosheet show charge and discharge capacities of 264.5 and 123.6 $mAhg^{-1}$ in the first cycle at 1 C, with a Coulombic efficiency of 47% [186]. Whereas r-GO/Ti_3C_2 heterostructures show the discharge capacity of 930 $mAhg^{-1}$, while its charge capacity is 500 $mAhg^{-1}$, with Coulombic efficiency more than 95% [187]. This significant improvement of r-GO/Ti_3C_2 over monolayer has also been reported by other groups [164, 188–192]. Recently, r-GO/Ti_2CT_r films significantly enhanced electrochemical performance with an improved reversible capacity of ≈700 $mAhg^{-1}$ at 0.1 Ag^{-1} with high Coulombic efficiency, excellent cycling stability and rate performance [187]. Moreover, the MoS_2@Ti_3C_2 nanocomposites give a reversible discharge capacity of 131.6 $mAhg^{-1}$ and corresponding a current density of 1000 $mAhg^{-1}$ for 200 cycles with excellent cycling stability, which is significantly higher than that of its pure Ti_3C_2 (58 $mAhg^{-1}$) and MoS_2 (3.6 $mAhg^{-1}$) [193]. Additionally, Ti_3C_2/CNTs heterostructure also show very high discharge and charge capacities of 642.5 and 403.5 $mAhg^{-1}$, respectively [194]. The Ti_3C_2/CNTs heterostructure not showed only high reversible capacity, but it has long cyclic stability and excellent rate capability [194].

Similarly, many researchers tried to improve the electrochemical performance, by forming free standing, flexible MXene/CNTs composite electrodes. Correspondingly, the specific capacity and resultant rate performance have been enhanced via improved ion accessibility. Nb_2CT_x could be effectively synthesized in

the presence of isopropylamine, as reported by Mashtalir and co-workers [17]. The free standing flexible Nb_2CT_x/CNT composite paper electrode gives an excellent cyclability, and Li-storage capacity of more than 400 $mAhg^{-1}$ at 0.5 C after 100 cycles and Coulombic efficiency is approximately 100% for anode materials. Especially in case of a full battery, when an Nb_2CT_x/CNT film used as an anode and a $LiFePO_4$ electrode as a cathode material then the charge and discharge capacity of 24 $mAhg^{-1}$ for Nb_2CT_x/CNT was reported for anode materials [195]. Apart from that, porous structure $Ti_3C_2T_x$/CNT films have been reported by Ren *et al* [190], in which significantly enhanced reversible storage capacity of lithium ions of ≈1250 $mAhg^{-1}$ at 0.1 C, good rate performance of 330 $mAhg^{-1}$ at 10 C, and excellent cycling stability was resulted. The free-standing and flexible $Ti_3C_2T_x$/CNT for Mg^{2+}/Li^{+} battery delivered a capacity of ≈100 $mAhg^{-1}$ at 0.1 C and ≈50 $mAhg^{-1}$ at 10 C. The capacity was maintained for >500 cycles at 80 $mAhg^{-1}$ at 1 C with Coulombic efficiency was very close to 100% [188]. The free-standing Mo_2CT_x/8 wt% CNT films, perform a stable reversible capacities of 250 and 76 $mAhg^{-1}$ at 5 and 10 Ag^{-1} over 1000 cycles for Li-ions as an electrode material, respectively [38].

Recently, MXene/oxides composite have been also used as an anode material for rechargeable batteries. The TiO_2 is a good candidate as an anode material for storage devices due to the low cost, environmental friendliness, and availability [196]. Researchers follow mainly two approaches, selectively partial oxidation of MXene and introduction of external metal ion to interpose oxides into MXene [197–201]. Ahmed *et al*[197] reported, TiO_2/Ti_2C hybrid materials delivered discharge capacities of 389, 337 and 297 $mAhg^{-1}$ at current densities of 100, 500 and 1000 mAg^{-1} at 50 cycles, respectively and it has excellent rate capability of 150 $mAhg^{-1}$ at 5000 mAg^{-1}. The $Nb_4C_3T_x$ containing external Nb_2O_5 nanoparticles ($Nb_4C_3T_x$@Nb_2O_5) were synthesized via CO_2 oxidation which gives a capacity of 208 mAg^{-1} at 0.25 C and the specific capacity of 94% with the Coulombic efficiency of 100% after 400 cycles [198]. As reported by Zhao *et al* [202], the hybrid structure $Ti_3C_2T_x$/$NiCo_2O_4$ used as an electrode achieved high reversible capacities of 1330, and 650 and 350 $mAhg^{-1}$ at 0.1, 5 and 10 C with stable over hundreds of cycles, respectively.

Furthermore, tin-based materials were used commonly as electrodes for LIBs due to the high capacities and environmental friendly [199–201]. According to Luo *et al* [200], the Sn^{4+} ion decorated Ti_3C_2 nanocomposites (PVP-Sn(IV)@Ti_3C_2) by liquid-phase immersion methods, give a good reversible volumetric capacity of 1375 mAh cm^{-3} (635 $mAhg^{-1}$) at 216.5 mA cm^{-3} (100 mAg^{-1}) after 50 cycles with a high current density of 6495 mA cm^{-3} (3 A g^{-1}) and these nanocomposites maintain after 100 cycles with a stable rate capacity of 504.5 mAh cm^{-3} (233 $mAhg^{-1}$), which is considerably higher than that of a graphite electrode (i.e. 550 mAh cm^{-3}). The Sn(IV) nanoparticle-modified Ti_3C_2 MXene (i.e. SnO_2-Ti_3C_2) hybrid structure synthesized via a hydrothermal method used as anode material for LIBs with excellent electrochemical performance. It shows the outstanding initial capacity of 1030.1 $mAhg^{-1}$ at 100 mAg^{-1}, and maintain 360 $mAhg^{-1}$ after 200 cycles [201].

Recently, Ti_3C_2 has been synthesized in the presence of NiCo-MOF (3D Ti_3C_2/NiCo-MOF composite structure). This significantly enhanced the electrochemical performance of Li-ion battery [222]. Ti_3C_2/NiCo-MOF composite structure was prepared by vacuum-assisted filtration technology as shown in figure 7(a). During the synthesis of this composite, when NiCo-MOF was added into Ti_3C_2 nanosheets solution via vacuum-assisted filtration, the porous structure was naturally constructed due to the interlayer hydrogen bonds between MXene and MOF nanostructure. The rate performance of Ti_3C_2/NiCo-MOF composite and bare Ti_3C_2 electrode at different current densities are presented in figure 7(b). It is evident that the bare Ti_3C_2 electrode displayed a charging capacity of 141 and 67 $mAhg^{-1}$ at the current density of 0.1 and 1 Ag^{-1}, respectively. It shows relatively low electrochemical performance for Li ion diffusion limited by compact stacking of multi-layer Ti_3C_2 structure [222]. On the other hand, the electrochemical performance of Ti_3C_2/NiCo-MOF composite structure is mainly depends on the loading of NiCo-MOF in the hybrid structure. The Ti_3C_2/NiCo-MOF-0.4 composite structure exhibits the a highest capacity of in all the considered compositions of NiCo-MOF loading and corresponding discharge capacity of 402 and 256 at the current density of 0.1 and 1 Ag^{-1}, respectively. The capacity maintains its initial value even at lower current density of 0.1 Ag^{-1}, it means that the Ti_3C_2/NiCo-MOF-0.4 composite electrode displayed excellent rate performance for a Li-ion battery. Figure 7(c), shows a high discharge capacity of 504.5 $mAhg^{-1}$ at the first cycle. The Ti_3C_2/NiCo-MOF-0.4 composite electrode displayed a relatively high capacity of 240 $mAhg^{-1}$ with the Coulombic efficiency of 85.7% after 400 cycles, claims excellent long cycling life as well as at a high rate. Another reported work by Meng *et al* [222], the $Ti_3C_2T_x$-based composite (figure 7(d)) anode in LIBs exhibits higher capacity and better rate performance than pristine $Ti_3C_2T_x$ nanostructure. Figure 7(e) manifests the specific capacity at different current density with various concentration of Si nanoparticles. During the rolling process to *in-situ* produces $Ti_3C_2T_x$/Si composite material with 10% silicon nanoparticles displayed the best overall enhancement among capacity, rate capability and cyclic stability for $Ti_3C_2T_x$ scrolls.

Table 3. Overview of electrochemical characteristics such as current rate (CR), reversible capacity (RC), cycle number (CN) and rate capability (RCap.) for MXene and MXene-based composite for Li-ions batteries.

Materials	CR	RC (mAg^{-1})	CN ($mAhg^{-1}$)	RCap.	Reference ($mAhg^{-1}$)
Ti_2CT_x	0.04 C	225	80	110	[113]
Ti_2C/TiO_2	100	389	100	280	[197]
Ti_3C_2/CNF	100	3320	2900	97	[203]
$Ti_3C_2T_x$/CNT	0.1 C	1250	100	500	[190]
$Nb_4C_3T_x$	100	380	1000	320	[204]
$Ti_3C_2T_x/NiCo_2O_4$	0.1 C	1330	100	1200	[202]
$SnO_2/Ti_3C_2T_x$	500	1041	50	451	[199]
$MoS_2@Ti_3C_2T_x$	50	843	200	132	[193]
Nb_2CT_x/CNT	0.1 C	420	100	370	[17]
Sn(IV)@Ti_3C_2	100	635	200	544	[200]
$Ti_3C_2T_x$/Ag	1 C	310	5000	260	[205]
$Ti_3C_2T_x$	30	100	50	—	[206]
$Ti_3C_2T_x$	200	203	500	140	[115]
$Ti_3C_2T_x$	1 C	134	100	106	[186]
Ti_3CNT_x	500	170	1000	—	[207]
$Hf_3C_2T_x$	200	137	200	47	[61]
Nb_2CT_x	1 C	170	150	—	[9]
V_2CT_x	1 C	260	150	—	[9]
$Nb_4C_3T_x$	50	208	400	—	[208]
$TiO_2/Ti_3C_2T_x$	200	267	2000	150	[115]
$TiO_2/Ti_3C_2T_x$	50	124	400	90	[208]
TiO_2/Ti_2CT_x	100	389	70	150	[197]
$Na_{0.23}TiO_2/Ti_3C_2T_x$	5000	178	4000	—	[209]
$Li_4Ti_5O_{12}$-$Ti_3C_2T_x$	5000	178	500	116	[210]
$Ti_3C_2T_x/Co_3O_4$	0.1 C	1200	100	—	[202]
$Fe_3O_4/Ti_3C_2T_x$	1 C	747	1000	—	[211]
PVP-Sn(IV)@$Ti_3C_2T_x$	500	544	200	—	[200]
$SnO_2/Ti_3C_2/HfO_2$	500	843	>50	258	[199]
$SnO_2/Ti_3C_2T_x$	100	400	200	360	[201]
$Ag/Ti_3C_2OH_{0.8}F_{1.2}$	1 C	310	5000	270	[205]
$MoS_2/Mo_aTiC_2T_x$	50	548	100	509	[212]
MoS_2/Ti_3C_2@C	200	1130	3000	—	[213]
rGO/$Ti_3C_2T_x$ film	50	221	275	150	[214]
rGO/$Ti_3C_2T_x$ foam	1000	179	1000	—	[215]
CNTs/Ti_3C_2	1000	430	300	—	[164]
$Ti_3C_2T_x$/CNTs	0.5 C	228	100	—	[17]
Mo_2C/CNT	400	560	70	—	[38]
Si@$Ti_3C_2T_x$	200	188	150	—	[216]
Ti_3C_2/Si@SiO_x@C	0.5 C	1444	1000	—	[217]
nSi@$Ti_3C_2T_x$	1500	2100	275	1280	[218]
nSi@Ti_3CNT_x	1500	1600	70	1100	[218]
Si@$Ti_3C_2T_x$	200	2118	100	—	[219]
3:2 Si@C:$Ti_3C_2T_x$	420	1700	150	—	[220]
1:1 $Ti_3C_2T_x$:Si	1 C	450	500	—	[221]

The hybrid structures are valuable to improve the reversible limit of MXene-based materials for the classical Li-storage system. These are the result of the development of two electrochemical responses (i.e. conversion/alloying for MXene based composites and adsorption-desorption for MXene network). The efficient and environmentally friendly route of intercalation of inorganic compounds with MXenes, such as the composites presented in table 3, should be adopted to further enhance the reversible capacity of the resultant batteries. Most of the MXene composites displayed significant improvement in gravimetric capacity, and it showed the maximum capacity higher than that of the typical graphite anodes [224], some even the excellent capacity of 2000 $mAhg^{-1}$ [203, 218, 219]. These composites also showed superior rate behavior and cycle lifetime. Furthermore, they exhibited quite strongly pseudo-capacitive cyclic voltammetry and charge–discharge profiles, which means that the significant portions of their capacities are delivered at higher voltages for conventional Li-ion battery anodes [190, 202, 203, 217–220]. From the above descriptions, it is clear that the rate capacity of MXenes is excellent and intrinsically connected to capacitive

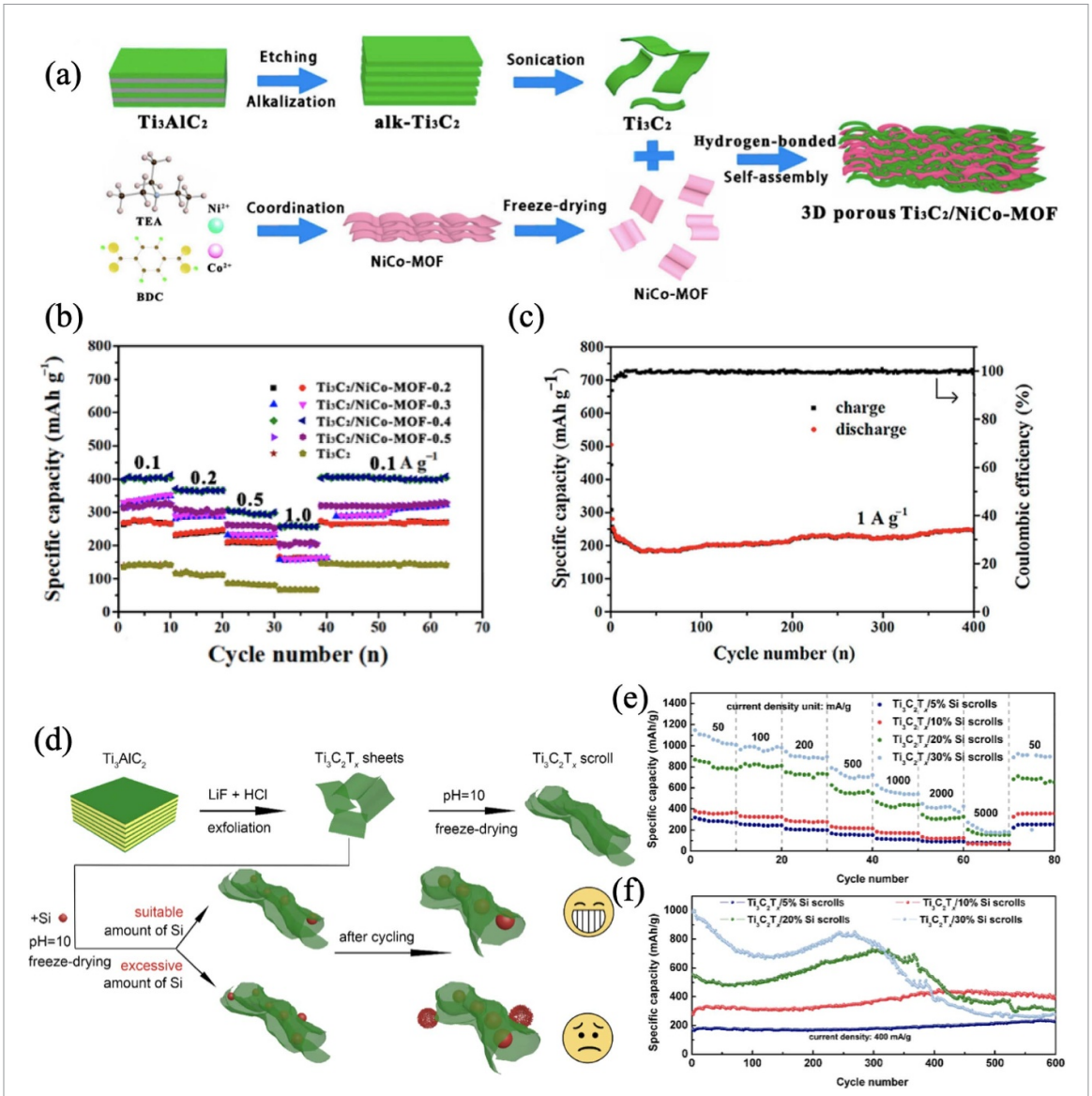

Figure 7. (a) Schematic illustration of the fabrication of 3D Ti_3C_2/NiCo-MOF composite structure, (b) rate performance at various current densities and (c) long cycling performance at the current density of 1.0 Ag^{-1} after 400 cycles of the Ti_3C_2/NiCo-MOF hybrid structure anode for the lithium-ion storage performance [223]. Reproduced from [223]. (d) The preparation method for $Ti_3C_2T_x$/Si composite structure, $Ti_3C_2T_x$ scrolls are used as the buffer matrix to accommodate Si nanoparticles, (e) rate profiles at the different current density, and (b) a high cycling performance at the current density of 400 mAg^{-1} [222]. Reproduced from [222]. Copyright 2020, Elsevier.

behavior [225]. Therefore, future work needs to optimize composite materials that exhibit fast redox peaks where MXenes contribute by providing conductive networks.

4.3. Non-lithium ions batteries

As described in earlier section, rechargeable batteries with non-lithium-ions such as Na^+, K^+, Mg^{2+}, Ca^{2+}, and Al^{3+} have received much attention as emerging low-cost and high energy-density technologies for large-scale renewable energy storage devices [19, 22, 23]. The hybrid structures i.e. MoS_2-intercalated $Ti_3C_2T_x$ composite produced using a hydrothermal route were presented to render an enhanced high specific capacity of 250.9 $mAhg^{-1}$ over 100 cycles, and rate performance with a capacity of 162.7 $mAhg^{-1}$ at 1 Ag^{-1} [245]. An isolated Ti_3C_2 system gives a specific capacity of 100 $mAhg^{-1}$ and a current density of 20 mAg^{-1} after 100 cycles [118]. Xie *et al* [189] reported that the porous MXene Ti_3C_2/CNTs films gave a high volumetric capacity of 345 $mAhcm^{-3}$ at 100 mAg^{-1} after 500 cycles and reversible capacity of 175 $mAhg^{-1}$ at 20 mAg^{-1} after 100 cycles. $Sb_2O_3/Ti_3C_2T_x$ hybrid structure sodium storage, delivered a rate performance of 295 $mAhg^{-1}$ at 2 Ag^{-1} and at 100 mAg^{-1} after 100 cycles enhanced the cycling performance up to 472 $mAhg^{-1}$ [230]. Some fruitful and enlightening attempts have been carried out to check the performance for practical applications of the full battery mechanism. Ti_3C_2/CNTs used as an anode and $Na_{0.44}MnO_2$ as a cathode powers a 2.5 V light-emitting diode for ≈25 min which expending an electrical energy of 41 μWh

Table 4. Overview of electrochemical characteristics such as current rate (CR), reversible capacity (RC), cycle number (CN) and rate capability (RCap.) from MXene and MXene-based composite for Na-ions batteries. Here, DMSO stands for dimethyl sulfoxide, NR-nanoribbons.

Materials	CR	RC (mAg^{-1})	CN ($mAhg^{-1}$)	RCap.	Reference ($mAhg^{-1}$)
$Ti_3C_2T_x$	200	79	500	—	[115]
$Ti_3C_2T_x$	200	178	500	105	[116]
$Ti_3C_2T_x$	100	101	500	—	[117]
$TiO_2/Ti_3C_2T_x$	200	267	2000	100	[115]
Ti_3CNT_x	10	90	100	75	[226]
$Hf_3C_2T_x$	50	68	200	47	[61]
S-doped-$Ti_3C_2T_x$	100	183	2000	121.3	[227]
TiO_2@$Ti_3C_2T_x$	30	220	5000	215	[228]
$CoNiO_2/Ti_3C_2T_x$	100	223	140	211	[229]
$SnS/Ti_3C_2T_x$	100	413	50	400	[117]
$Sb_2O_3/Ti_3C_2T_x$	200	450	100	–	[230]
$DMSO/Ti_3C_2T_x$	100	120	500	100	[231]
Crumpled $Ti_3C_2T_x$	20	250	50	120	[232]
Alkalized $Ti_3C_2T_x$ NR	20	167	500	—	[233]
Mo_2CT_x spheres	50	370	1000	—	[163]
$Ti_3C_2T_x$ spheres	50	330	1000	—	[163]
V_2CT_x spheres	50	340	1000	—	[163]
Ti_3CNT_x spheres	20	154	100	75	[226]

Table 5. Overview of theoretical electrochemical performances of MXenes and MXene-based composite as electrode active material for metal-ions batteries.

Materials	Applications	Capacity ($mAhg^{-1}$)	Reference
$Ti_3C_2T_x$	LIBs	447.8	[234]
Ti_2CO_2/graphene	LIBs	426	[235]
Ti_3C_2	SIBs	351.8	[234]
Y_2C	SIBs	564	[236]
Ti_3C_2	KIBs	191.8	[234]
Ti_2CO_2/graphene	KIBs	209.8	[237]
V_2CO_2/graphene	KIBs	207.22	[237]
Zr_2CO_2	KIBs	474	[238]
$Zr_3C_2O_2$	KIBs	326	[238]
Ti_2CO_2	LIBs	383	[114]
$Ti_3C_2O_2$	LIBs	268	[114]
V_2CO_2	LIBs	367	[114]
Nb_2CO_2	LIBs	233	[114]
Ti_3C_2	LIBs	320	[114]
Ti_2N_2	LIBs/SIBs/KIBs/ MIBs/CIBs/AIBs	484/484/242/ 2930/488/45	[239]
Ti_2NO_2	LIBs/SIBs/KIBs/ MIBs/CIBs/AIBs	378/378/378/ 2269/756/1134	[239]
Ti_2NF_2	LIBs/SIBs/KIBs	90/181/181	[239]
$VS_2/Mo_2CO_2Na_5$	SIBs	420.09	[240]
$VS_2/Nb_2CO_2Na_5$	SIBs	428.29	[240]
$VS_2/Ti_2CO_2Na_5$	SIBs	601.44	[240]
$VS_2/V_2CO_2Na_5$	SIBs	585.29	[240]
Sc_2CO_2	LIBs/graphene	229.85	[241]
$Sc_2C(OH)_2$/graphene	LIBs	227.87	[241]
Ti_2CO_2/graphene	LIBs	234.39	[241]
$Ti_2C(OH)_2$/graphene	LIBs	232.34	[241]
V_2CO_2/graphene	LIBs	234.12	[241]
$V_2C(OH)_2$/graphene	LIBs	232.07	[241]
Cr_2CO_2	LIBs/SIBs/KIBs/ MIBs/CIBs/AIBs	331/276/239/ 545/470/796	[242]
Mo_2C	LIBs/SIBs	263/263	[243]
Zr_2C	LIBs	310	[244]
$Zr_3C_2S_2$	LIBs	259	[244]

[189]. During the full cell mechanism, Ti_3C_2/CNT-SA electrode gives the charge and discharge capacities of 270 and 286 $mAhcm^{-3}$ respectively. The corresponding volumetric discharge capacity was retained as 242

mAhcm^{-3} at the current density of 50 mAg^{-1} after 60 cycles with a Coulombic efficiency of 99% [246]. Ti_3C_2 monolayer displayed fast migration of K-ion with specific capacity of 191.8 mAhg^{-1} using DFT in theoretical investigations by Dequan *et al* [234].

While Zhao *et al* synthesized PDDC-N-rich porous carbon nanochips (NPCN)/Ti_3C_2 a hybrid structure which exhibited a good rate performance as shown in figure 8. The PDDC-NPCN/Ti_3C_2 hybrid structure is prepared in face-to-face manner by the electrostatic interaction between NPCN and multiple layers of Ti_3C_2 (see figure 8(a)). The PDDC-NPCN/Ti_3C_2 hybrid structure displayed a layered structure with large surface area and effectively utilize two components and more accessible active sites which can confirm the nearby contact between PDDC-NPCN and Ti_3C_2. The galvanostatic charge/discharge profiles of the PDDC-NPCN/Ti_3C_2 hybrid structure anode are measured at the current density of 0.1 Ag^{-1} for initial first five cycles. The initial discharge capacity of 797.3 mAhg^{-1} and charge capacities of 583.6 mAhg^{-1} achieved as presented in figure 8(b). From figure 8(c), it is confirmed that the PDDC-NPCN/Ti_3C_2 hybrid structure anode exhibits superior rate performance at high current densities. Also, it shows high reversible capacity of 358 mAhg^{-1} at the current density of 0.1 Ag^{-1} even after 300 cycles while after 2000 cycles at the current density of 1.0 Ag^{-1}, it displayed a reversible capacity of 252 mAhg^{-1} with a decay rate of only 0.03 per cycle (figure 8(d)). From XRD pattern, the diffraction peak (001) of Ti_3C_2 shifted to a lower angle and representing that the interlayer spacing expanded from 19.2 to 24.6 Å, which corresponds to the K^+ intercalation into the PDDC-NPCN/Ti_3C_2 composite anode. The hybrid structures provide a larger interlayer spacing which makes a 3D interconnected conductive framework to accelerate the ion/electron transfer rate. PDDC-NPCN/Ti_3C_2 composite also shows a high chemical stability due to its good tolerance toward volume change caused by phase change in fast charge and discharge process. Additionally, it was seen that the PDDC-NPCN/Ti_3C_2 composite material significantly reduces the K^+ binding strength, which accelerates reaction kinetics. PDDC-NPCN/Ti_3C_2 composite material exhibits high inter-layer spacing, providing significant capacity, excellent cycle performance, excellent speed performance, and exceptionally good speed capacity for K-ion battery. These theoretical and experimental results proposed a new strategy to prepare a high performance MXene-based composite material for K-ion battery anode.

To summarize, MXene heterostructures (MXenes composite) can accommodate metal ions due to their wide interlayer spacing, where graphite have lower spacing which does not prefer heavier ion intercalation [234, 235, 237, 238]. Although, in the case of full intercalations, the diffusion rates are limited, and in this case, an increase in the interlayer spacing of MXenes and their composites is needed. The performance of metal ions batteries are summarized in tables 4 and 5 in which $Sb_2O_3/Ti_3C_2T_x$ composite electrode displayed high performance by Guo and co-workers [230]. Overall the MXenes heterostructures (e.g. MXene combine with graphene or other layered materials) have lower diffusion barriers for alkali metals than MXene or isolated graphene [235, 237].

4.4. Lithium–sulfur battery

Li–S batteries have garnered much attention owing to the simple configurations, high energy density and capacity and more environmentally friendly as described in previous section. Hybrid structures and composites also enhance the properties of materials toward Li–S battery applications. As reported by Peng *et al* [250], hybrid structure TiC@G/S as cathode for Li–S battery shows without binder, separator, and current collector capacity of 670 mAhg^{-1} at a current density of 0.2 C after 100 cycles with Coulombic efficiency of 95%. Generally, a typical cathode for Li–S battery is made by carbon/sulfur. According to Zhao *et al* [251], the multilayers of carbon/sulfur flakes derived from MXene Ti_2SC displayed promising characteristics for Li–S battery. The fabricated Lamellar structured, flexible Ti_3C_2 MXene (graphene, BN) lithium film anode have low overpotential, exhibited high reversible capacity of 841 mAhg^{-1} after 100 cycles. A lithium–sulfur full cell with Ti_3C_2-Li as anode and sulfur–carbon as cathode exhibited a high energy density and excellent cycle performances [252].In another case, MXene nanosheets with hydroxyl group/CNTs composites were recently synthesized [123] and provided high polysulfide adsorption. This further enabled sulfur hosts with excellent long-term cycling performance, with reversible capacities of ≈450 mAhg^{-1} at 0.5 C after 1200 cycles with a capacity retention of ≈95% [123]. 3D $Ti_3C_2T_x$/rGO/sulfur composites used as a cathode host material for Li–S battery prepared by using a liquid phase impregnation technique provided a high initial capacity of 1144.2 mAhg^{-1} at 0.5 C with a high level of capacity retention of 878.4 after 300 cycles [253].

Gao and co-workers [248] synthesized the TiO_2 QDs decorated on the surface of $Ti_3C_2T_x$ MXene (see figure 9(a)(I)) has a quite promising electrochemical performance as a sulfur host for achieving fast and stable Li–S batteries. The TiO_2 QDs/MXene hybrid structure exhibit superior performance suppressing the shuttling effect with polysulfides which gives excellent long-term cyclability and rate capability as presented in figure 9(a). Compared with a MXene/S cathode which displayed a lower discharging voltage (2.03–2.31 V), TiO_2 QDs/MXene delivered a slightly higher voltage (2.09–2.38 V) which described the reduction of

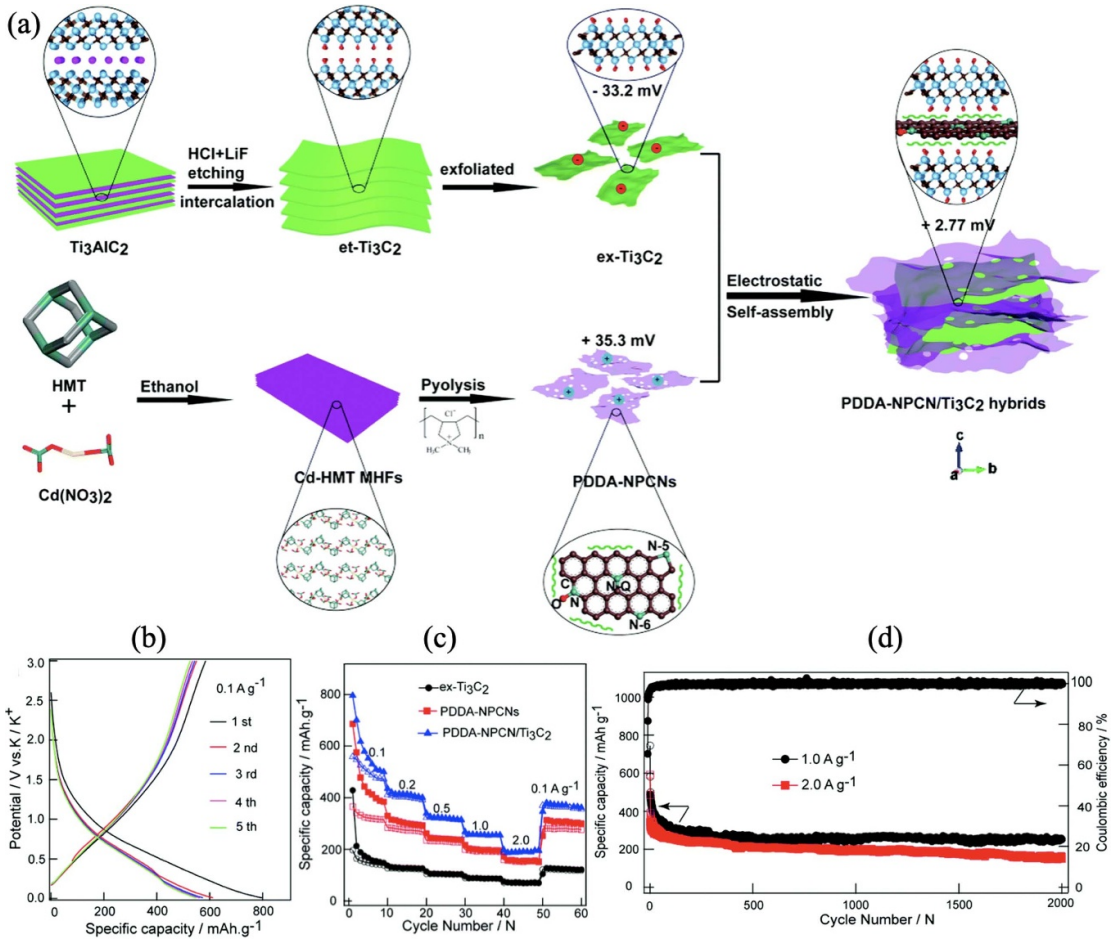

Figure 8. (a) Schematic representation of the fabrication of PDDC-NPCN/Ti_3C_2 hybrid structure, (b) initial galvanostatic charge/discharge profiles at the current density of 0.1 Ag^{-1}, (c) rate performance at different current densities and (d) long cycling performance at the current density of 1.0 and 2.0 Ag^{-1} after 2000 cycles of the PDDC-NPCN/Ti_3C_2 hybrid structure anode for the potassium-ion storage performance. Reproduced from [247]. Copyright 2020, Royal Society of Chemistry.

elemental sulfur to higher-order polysulfides (Li_2S_n, $4 \leq n \leq 8$). In contrast, the plateau at the lower voltage for these two cases is related to the reduction process of higher-order to lower-order lithium polysulfides [254]. The TiO_2 QDs/MXene hybrid structure exhibited higher capacities of 1158, 1037, 925, 812 and 663 $mAhg^{-1}$ at C/5, C/2, 1 C, 2 C and 5 C current densities, respectively, where 1 C = 1675 mAg^{-1} as presented in figure 9(a)(III). Figure 9(a) (IV) displays the long-term cyclability of TiO_2 QDs/MXene composite, which shows the high capacity of 680 $mAhg^{-1}$ at 2 C after 500 cycles with sulfur loading of 1.5 mg cm^{-2} and this value is significantly twice that of MXene/S cathodes. The Coulombic efficiency of TiO_2 in QDs/MXene composite cathodes reaches nearly 100% in the whole cycling process. More importantly, superior electrochemical performance could be available at higher sulfur loading of 5.5 mg cm^{-2}. Another reported work on $Ti_3C_2T_x/MnO_2$ composites delivered a high initial capacity of 1140 $mAhg^{-1}$ at 0.2 C after 500 cycles [158]. Table 2 displayed the summarized lists of cathode materials for Li–S batteries.

Another fascinating work by Lv *et al* [249], the highly conductive Mo_2CT_x/CNT composites has been synthesized via a ball milling procedure (figure 9(b)(I)). The Mo_2CT_x/CNT composite electrode exhibited superior electrochemical performance in the terms of good rate capability, high capacity and high initial reversible capacity of 1314, 1068 and 959 $mAhg^{-1}$ at different sulfur loading of 1.8, 3.5 and 5.6 mg cm^{-2}, respectively (figure 9(b)(II)). Furthermore, the rate capacities of Mo_2CT_x/CNT/S electrode and their comparison with Mo_2CT_x/S at various current densities of 0.1 to 5 C are displayed in figure 9(b)(III). The charging-discharging profile for Mo_2CT_x/CNT/S and Mo_2CT_x/S composites is displayed in figure 9(b)(IV). The Mo_2CT_x/CNT composites exhibited the reversible capacities of 954 at 1 C after 100 cycles with ≈100% Coulombic efficiency which shows excellent electrochemical performance. MXenes and MXenes composites can capture the soluble LiPSs though a strong transition metal and sulfur interaction to suppress the shuttling effect. Also, functionalized MXenes surface displays strong chemisorption to LiPSs and thus significantly reduces the active material loss and provide high capacities after long-term cycling. Based on the

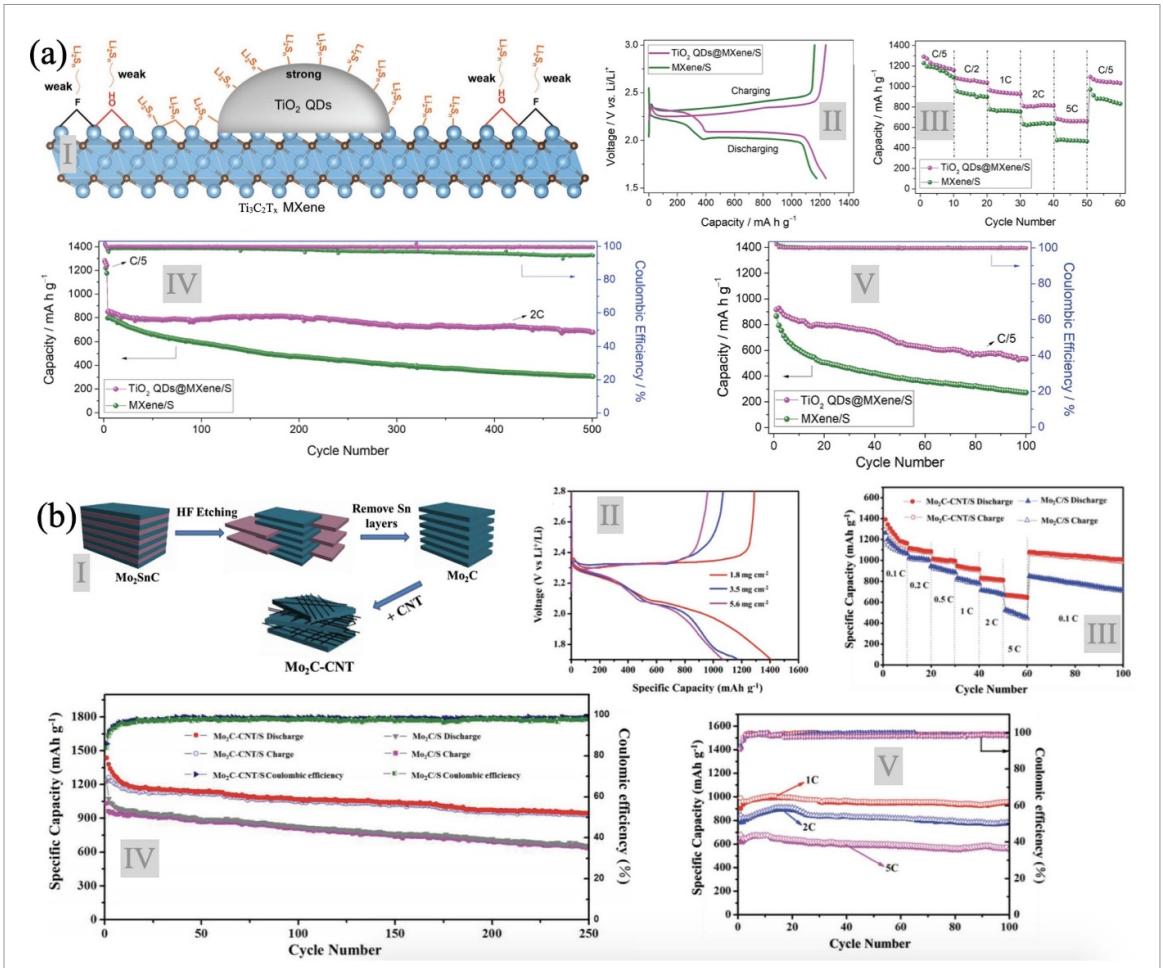

Figure 9. (a)(I) Schematic representations of the shuttling effect of polysulfides on the surface of $Ti_3C_2T_x$ MXene/TiO_2 heterostructure, (II) the charging-discharging profile at C/5, (III) rate capabilities at various current densities, (IV) cycle performance at 2 C (with sulfur loading of 1.5 mg cm^{-2}) of TiO_2 QDs/MXene/S and MXene/S cathodes, and (V) the comparisons of electrochemical performance at C/5 (with sulfur loading of 5.5 mg cm^{-2}) of TiO_2 QDs/MXene/S and MXene/S cathodes. Reproduced with permission [248]. Copyright 2018, Wiley-VCH. b(I) Schematic illustration of the growth routine of Mo_2CT_x/CNT heterostructure, (II) initial charging/discharging curves of Mo_2CT_x/CNT cells under various sulfur loadings, (III) Rate capability of the Mo_2C/CNT/S and Mo_2C/S at various current densities, (IV) Cycling performances of the Mo_2C/CNT/S and Mo_2C/S at 0.1 C, and (V) Cycling stability of Mo_2C/CNT/S cells at 1, 2, and 5 C. Reproduced with permission [249]. Copyright 2019, Wiley-VCH.

summarized lists of composites materials in all the tables, heterostructures proved to be promising candidates for energy storage applications.

5. Summary and outlook

Three types of MXenes, namely 2D metal carbides, 2D metal nitrides, and 2D metal carbonitrides with different surface functional group such as oxygen (–O), hydroxyl (OH) and/or fluorine (–F) were fabricated in last decade by selective etching and exfoliation of MAX phases. High surface charge and hydrophilicity of the MXenes lead to stable water-based colloidal arrangements that do not require surfactants for adjustment. This makes MXene synthesis and processing cheap and straightforward, which further encourages researchers to investigate their potential applications. To date, the continuous increase in the interest of electrochemical energy storage devices require further investigation and development of enhanced electrode materials, which can increase the loading of ions and molecules with high capacity and faster kinetics. From this viewpoint, a new smart 2D electrode material Ti_3C_2 MXene was reported and investigated in 2011. Furthermore, many other 2D MXenes exhibit attractive electronic, optical, photonic, photocatalyst, and thermoelectric properties. Apart from this, it has superior attributes for electrochemical such as high strength, high melting point, high electrical and thermal conductivity, oxidation resistance, hydrophilic nature, compositional variability, and large surface area. Therefore, MXenes have evolved as an alternative for advanced electrode materials. The MXene layers have large interlayer spacing, which is advantageous for different sized cations, to be easily intercalated into the layers. The combination of superior electrical conductivity and mechanical strength and their functionalized surface by oxide and/or hydroxide, including

uncovered redox-active transition metal atom, make MXenes alluring for the utilization as battery electrodes. Mxenes exhibit high capacity and stability for Li- batteries. Besides lithium, there are several cations such as sodium (Na), potassium (K), magnesium (Mg), that intercalated in the MXenes layers and served as promising candidates for energy devices applications. The intercalation of the larger size of some cations has not been explored because there can be a propensity for large interlayer cations to lead to low conductivity, hence, it will influence the charge transfer and diffusion kinetics of the ions.

The present review summarizes the structural and electronic properties of bulk MAX phases and then their 2D counterparts MXenes along with the synthesis methods of precursors and exfoliation of nanoflakes. The applications of MXenes and MXenes composites/hybrid structures have been discussed in detail for and alkali-ion and Li–S batteries. The outstanding features makes MXenes outlier from other 2DMs families and make them promising candidates for high-performance electrodes. In particular, MXenes and its composites have many advantages for Li–S batteries, such as the unique layered structure of MXenes with the appropriate surface area for sulfur/sulfides, which provides excellent mechanical strength to resist the stress induced by large volume expansion of sulfur. The metallic conductivity facilitates the electron transport kinetics through the electrolyte/electrode interface, improves electrode polarization, and assists high rate responses even at a high sulfur loading. MXenes have been used both as sulfur hosts and modified spacers and the electrochemical performance of Li–S batteries based on MXene can improve mainly through the materials and design of the cell. It can be achieved by increasing active sites of interaction to strengthen immobilizing Li_2Sn, introducing spacers to suppress the restacking of nanosheet and building 3D structures to improve sulfur loading, and so on. Surface chemistry plays a essential role in accomplishing electrodes with a superior affinity for LiPSs species. The functionalization of MXenes reduces the strong form of metal–sulfur bonds for LIPS's species, and further enhances the Li-ion diffusivity on the surface, leading to excellent electrochemical performance. Furthermore, advantages of MXenes and its composites have been discussed for restacking, stability, high electrical conductivity, and fast electron/ion transfer, which open new research windows in the fields of energy conversion and storage applications. However, some of the MXenes composites with the conducting polymers are yet to be investigated. These possible MXenes hybrid structures may contribute to the field of potential applications in the next generations of battery electrodes. There are wide open challenges for controlled synthesis MXenes and MXenes composites for practical applications. New synthesis methods is needed for controlled synthesis of functionalized MXenes, as of current methods lead to random functionalization with more than one functional groups [255]. Rapid oxidation of MXene is a well known problem to be taken care of before its utilization in any commercial products such as energy production, conversion and storage applications.

Acknowledgments

DS and RA thanks Olle Engkvists Stiftelse (198-0390), Carl Tryggers Stiftelse for Vetenskaplig Forskning (CTS:18:4) and Swedish Research Council (VR-2016-06014) for financial support. VS acknowledges the SSF grant (ITM17-0324) for financial support. NK and AA acknowledge the PPR2 project: (MISTERSFC-CNRST) for financial support. SNIC and HPC2N are acknowledged for providing the computing facilities.

Authors contribution

DS, VS and NK have equally contributed in this review article. AA and RA has helped to improve the scientific content of the review article. RA has conceptualized, supervised, facilitate resources and funding for this work.

ORCID iDs

Deobrat Singh https://orcid.org/0000-0001-7246-8743
Vivekanand Shukla https://orcid.org/0000-0001-7724-6357
Nabil Khossossi https://orcid.org/0000-0002-3914-4162
Rajeev Ahuja https://orcid.org/0000-0003-1231-9994

References

[1] Zhu Y, Murali S, Cai W, Li X, Suk J W, Potts J R and Ruoff R S 2010 *Adv. Mater.* **22** 3906–24
[2] Vogt P, De Padova P, Quaresima C, Avila J, Frantzeskakis E, Asensio M C, Resta A, Ealet B and Le Lay G 2012 *Phys. Rev. Lett.* **108** 155501

[3] Derivaz M, Dentel D, Stephan R, Hanf M C, Mehdaoui A, Sonnet P and Pirri C 2015 *Nano Lett.* **15** 2510–16
[4] Brent J R, Savjani N, Lewis E A, Haigh S J, Lewis D J and O'Brien P 2014 *Chem. Commun.* **50** 13338–41
[5] Wang Q H, Kalantar-Zadeh K, Kis A, Coleman J N and Strano M S 2012 *Nat. Nanotechnol.* **7** 699
[6] Sun Z, Liao T, Dou Y, Hwang S M, Park M S, Jiang L, Kim J H and Dou S X 2014 *Nat. Commun.* **5** 3813
[7] Naguib M, Kurtoglu M, Presser V, Lu J, Niu J, Heon M, Hultman L, Gogotsi Y and Barsoum M W 2011 *Adv. Mater.* **23** 4248–53
[8] Naguib M, Mashtalir O, Carle J, Presser V, Lu J, Hultman L, Gogotsi Y and Barsoum M W 2012 *ACS Nano* **6** 1322–31
[9] Naguib M, Halim J, Lu J, Cook K M, Hultman L, Gogotsi Y and Barsoum M W 2013 *J. Am. Chem. Soc.* **135** 15966–9
[10] Khazaei M, Arai M, Sasaki T, Chung C Y, Venkataramanan N S, Estili M, Sakka Y and Kawazoe Y 2013 *Adv. Funct. Mater.* **23** 2185–92
[11] Anasori B, Xie Y, Beidaghi M, Lu J, Hosler B C, Hultman L, Kent P R, Gogotsi Y and Barsoum M W 2015 *ACS Nano* **9** 9507–16
[12] Gogotsi Y 2015 *Nat. Mater.* **14** 1079–80
[13] Naguib M, Mochalin V N, Barsoum M W and Gogotsi Y 2014 *Adv. Mater.* **26** 992–1005
[14] Deysher G *et al* 2019 *ACS Nano* **14** 204–17
[15] Verger L, Xu C, Natu V, Cheng H M, Ren W and Barsoum M W 2019 *Current Opin. Solid State Mater. Sci.* **23** 149–63
[16] Liu F, Zhou A, Chen J, Jia J, Zhou W, Wang L and Hu Q 2017 *Appl. Surf. Sci.* **416** 781–9
[17] Mashtalir O, Lukatskaya M R, Zhao M Q, Barsoum M W and Gogotsi Y 2015 *Adv. Mater.* **27** 3501–6
[18] Anasori B, Lukatskaya M R and Gogotsi Y 2017 *Nat. Rev. Mater.* **2** 1–17
[19] Greaves M, Barg S and Bissett M A 2020 *Batteries Supercaps* **3** 214–35
[20] Xiao Z, Li Z, Meng X and Wang R 2019 *J. Mater. Chem.* A **7** 22730–43
[21] Yang J, Bao W, Jaumaux P, Zhang S, Wang C and Wang G 2019 *Adv. Mater. Interfaces* **6** 1802004
[22] Aslam M K, Niu Y and Xu M 2020 *Adv. Energy Mater.* 2000681
[23] Dong Y, Shi H and Wu Z S 2020 *Adv. Funct. Mater.* **30** 2000706
[24] Prasad C, Yang X, Liu Q, Tang H, Rammohan A, Zulfiqar S, Zyryanov G V and Shah S 2020 *J. Ind. Eng. Chem.* **85** 1–33
[25] Karahan H E *et al* 2020 *Adv. Mater.* **32** 1906697
[26] Zhang X, Zhang Z and Zhou Z 2018 *J. Energy Chem.* **27** 73–85
[27] Tang H, Hu Q, Zheng M, Chi Y, Qin X, Pang H and Xu Q 2018 *Progress Nat. Sci.: Mater. Int.* **28** 133–47
[28] Zhu J *et al* 2017 *Coord. Chem. Rev.* **352** 306–27
[29] Pang J, Mendes R G, Bachmatiuk A, Zhao L, Ta H Q, Gemming T, Liu H, Liu Z and Rummeli M H 2019 *Chem. Soc. Rev.* **48** 72–133
[30] Jiang X, Kuklin A V, Baev A, Ge Y, Ågren H, Zhang H and Prasad P N 2020 *Phys. Rep.* **848** 1–58
[31] Nowotny V H 1971 *Prog. Solid State Chem.* **5** 27–70
[32] Barsoum M W and El-Raghy T 1996 *J. Am. Ceram. Soc.* **79** 1953–6
[33] Barsoum M W 2000 *Prog. Solid State Chem.* **28** 201–81
[34] Barsoum M W and El-Raghy T 2001 *Am. Sci.* **89** 334–43
[35] Barsoum M W 2013 *MAX Phases: Properties of Machinable Ternary Carbides and Nitrides* (New Jersey: John Wiley & Sons)
[36] Karlsson L H, Birch J, Halim J, Barsoum M W and Persson P O 2015 *Nano Lett.* **15** 4955–60
[37] Meshkian R, Näslund L k, Halim J, Lu J, Barsoum M W and Rosen J 2015 *Scr. Mater.* **108** 147–50
[38] Halim J *et al* 2016 *Adv. Funct. Mater.* **26** 3118–27
[39] Zhan C, Sun W, Xie Y, Jiang D e and Kent P R 2019 *ACS App. Mater. Interfaces* **11** 24885–905
[40] Liu Z, Zheng L, Sun L, Qian Y, Wang J and Li M 2014 *J. Am. Ceram. Soc.* **97** 67–9
[41] Khazaei M, Ranjbar A, Arai M, Sasaki T and Yunoki S 2017 *J. Mater. Chem.* C **5** 2488–503
[42] Khazaei M, Arai M, Sasaki T, Estili M and Sakka Y 2014 *J. Phys.: Condens. Matter.* **26** 505503
[43] Guo Z, Zhou J, Si C and Sun Z 2015 *Phys. Chem. Chem. Phys.* **17** 15348–54
[44] Sarikurt S, Çakr D, Keçeli M and Sevik C 2018 *Nanoscale* **10** 8859–68
[45] Magne D, Mauchamp V, Célérier S, Chartier P and Cabioc'h T 2015 *Phys. Rev.* B **91** 201409
[46] Anasori B *et al* 2015 *J. Appl. Phys.* **118** 094304
[47] Barsoum M W and Radovic M 2011 *Ann. Rev. Mater. Res.* **41** 195–227
[48] Ghidiu M, Lukatskaya M R, Zhao M Q, Gogotsi Y and Barsoum M W 2014 *Nature* **516** 78–81
[49] Hoffman E N, Yushin G, El-Raghy T, Gogotsi Y and Barsoum M W 2008 *Microporous Mesoporous Mater.* **112** 526–32
[50] Gupta S and Barsoum M 2011 *Wear* **271** 1878–94
[51] Gusmao R, Sofer Z and Pumera M 2017 *Angewandte Chemie Int. Edn* **56** 8052–72
[52] Stankovich S, Dikin D A, Piner R D, Kohlhaas K A, Kleinhammes A, Jia Y, Wu Y, Nguyen S T and Ruoff R S 2007 *Carbon* **45** 1558–65
[53] Eda G, Yamaguchi H, Voiry D, Fujita T, Chen M and Chhowalla M 2011 *Nano Lett.* **11** 5111–16
[54] Khossossi N, Singh D, Ainane A and Ahuja R 2020 *Chemi. Asian J.* **15** 3390
[55] Ng V M H, Huang H, Zhou K, Lee P S, Que W, Xu J Z and Kong L B 2017 *J. Mater. Chem.* A **5** 3039–68
[56] Zhan X, Si C, Zhou J and Sun Z 2020 *Nanoscale Horizons* **5** 235–58
[57] Wang X and Zhou Y 2010 *Journal of Mater. Sci. Technol.* **26** 385–416
[58] Ghidiu M *et al* 2014 *Chem. Commun.* **50** 9517–20
[59] Soundiraraju B and George B K 2017 *ACS Nano* **11** 8892–900
[60] Zhou J, Zha X, Chen F Y, Ye Q, Eklund P, Du S and Huang Q 2016 *Angewandte Chemie Int. Edn* **55** 5008–13
[61] Zhou J *et al* 2017 *ACS Nano* **11** 3841–50
[62] Tao Q *et al* 2017 *Nat. Commun.* **8** 1–7
[63] Persson I *et al* 2018 *Small* **14** 1703676
[64] Ronchi R M, Arantes J T and Santos S F 2019 *Ceram. Int.* **45** 18167–88
[65] Liu F, Zhou J, Wang S, Wang B, Shen C, Wang L, Hu Q, Huang Q and Zhou A 2017 *J. Electrochem. Soc.* **164** A709–A713
[66] Halim J *et al* 2014 *Chem. Mater.* **26** 2374–81
[67] Yang S, Zhang P, Wang F, Ricciardulli A G, Lohe M R, Blom P W and Feng X 2018 *Angewandte Chemie* **130** 15717–21
[68] Li T *et al* 2018 *Angewandte Chemie Int. Edn.* **57** 6115–19
[69] Li M *et al* 2019 *J. Am. Chem. Soc.* **141** 4730–7
[70] Alhabeb M, Maleski K, Mathis T S, Sarycheva A, Hatter C B, Uzun S, Levitt A and Gogotsi Y 2018 *Angewandte Chemie Int. Edn.* **57** 5444–8
[71] Urbankowski P *et al* 2016 *Nanoscale* **8** 11385–91

[72] Urbankowski P, Anasori B, Hantanasirisakul K, Yang L, Zhang L, Haines B, May S J, Billinge S J and Gogotsi Y 2017 *Nanoscale* **9** 17722–30
[73] Mashtalir O, Naguib M, Mochalin V N, Dall'Agnese Y, Heon M, Barsoum M W and Gogotsi Y 2013 *Nat. Commun.* **4** 1–7
[74] Alhabeb M, Maleski K, Anasori B, Lelyukh P, Clark L, Sin S and Gogotsi Y 2017 *Chem. Mater.* **29** 7633–44
[75] Omomo Y, Sasaki T, Wang L and Watanabe M 2003 *J. Am. Chem. Soc.* **125** 3568–75
[76] Naguib M, Unocic R R, Armstrong B L and Nanda J 2015 *Dalton Trans.* **44** 9353–8
[77] Anasori B and Gogotsi Y 2019 *2D Metal Carbides and Nitrides (Mxenes)* (Berlin: Springer)
[78] Shukla V, Araujo R B, Jena N K and Ahuja R 2017 *Nano Energy* **41** 251–60
[79] Rasmussen F A and Thygesen K S 2015 *J. Phys. Chem.* **119** 13169–83
[80] Lin C, Zhang X and Rao Z 2017 *Nano Energy* **38** 249–56
[81] Kuklin A V, Kuzubov A A, Kovaleva E A, Mikhaleva N S, Tomilin F N, Lee H and Avramov P V 2017 *Nanoscale* **9** 621–30
[82] Eklund P, Dahlqvist M, Tengstrand O, Hultman L, Lu J, Nedfors N, Jansson U and Rosén J 2012 *Phys. Rev. Lett.* **109** 035502
[83] Frey N C, Wang J, Vega Bellido G I, Anasori B, Gogotsi Y and Shenoy V B 2019 *ACS Nano* **13** 3031–41
[84] Wang J, Zhou Y, Liao T and Lin Z 2007 *J. Mater. Res.* **22** 2685–90
[85] Hantanasirisakul K and Gogotsi Y 2018 *Adv. Mater.* **30** 1804779
[86] Shukla V, Jena N K, Naqvi S R, Luo W and Ahuja R 2019 *Nano Energy* **58** 877–85
[87] Naqvi S R, Shukla V, Jena N K, Luo W and Ahuja R 2020 *App. Mater. Today* **19** 100574
[88] Liang Y, Khazaei M, Ranjbar A, Arai M, Yunoki S, Kawazoe Y, Weng H and Fang Z 2017 *Phys. Rev.* B **96** 195414
[89] Venkateshalu S, Cherusseri J, Karnan M, Kumar K S, Kollu P, Sathish M, Thomas J, Jeong S K and Grace A N 2020 *ACS Omega* **5** 17983–92
[90] Eklund P, Beckers M, Jansson U, Högberg H and Hultman L 2010 *Thin Solid Films* **518** 1851–78
[91] Handoko A D, Steinmann S N and Seh Z W 2019 *Nanoscale Horizons* **4** 809–27
[92] Khazaei M, Ranjbar A, Liang Y and Yunoki S 2019 Electronic properties and applications of MXenes from ab initio calculations perspective *2D Metal Carbides and Nitrides (Mxenes)* (Berlin: Springer) pp 255–89
[93] Lipatov A and Sinitskii A 2019 Electronic and mechanical properties of MXenes derived from single-flake measurements *2D Metal Carbides and Nitrides (Mxenes)* (Berlin: Springer) pp 301–25
[94] Wang Y, Xu Y, Hu M, Ling H and Zhu X 2020 *Nanophotonics* **1**
[95] Kim S J *et al* 2018 *ACS Nano* **12** 986–93
[96] Toth L 2014 *Transition Metal Carbides and Nitrides* (Amsterdam: Elsevier)
[97] Xie Y and Kent P 2013 *Phys. Rev.* B **87** 235441
[98] Zhao S, Kang W and Xue J 2014 *Appl. Phys. Lett.* **104** 133106
[99] Lee Y, Cho S B and Chung Y C 2014 *ACS App. Mater. Interfaces* **6** 14724–8
[100] Lee Y, Hwang Y, Cho S B and Chung Y C 2014 *Phys. Chem. Chem. Phys.* **16** 26273–8
[101] Li L 2016 *J. Phys. Chem.* **120** 24857–65
[102] Hantanasirisakul K, Zhao M Q, Urbankowski P, Halim J, Anasori B, Kota S, Ren C E, Barsoum M W and Gogotsi Y 2016 *Adv. Electron. Mater.* **2** 1600050
[103] Lipatov A, Alhabeb M, Lukatskaya M R, Boson A, Gogotsi Y and Sinitskii A 2016 *Adv. Electron. Mater.* **2** 1600255
[104] Guo J, Wang J, Wu Z, Lei W, Zhu J, Xia K and Wang D 2017 *J. Mater. Chem.* A **5** 4879–85
[105] Enyashin A N and Ivanovskii A L 2013 *J. Phys. Chem.* **117** 13637–43
[106] Dong L, Kumar H, Anasori B, Gogotsi Y and Shenoy V B 2017 *J. Phys. Chem. Lett.* **8** 422–8
[107] Sun W, Xie Y and Kent P R 2018 *Nanoscale* **10** 11962–8
[108] Tan T L, Jin H M, Sullivan M B, Anasori B and Gogotsi Y 2017 *ACS Nano* **11** 4407–18
[109] Khazaei M, Wang V, Sevik C, Ranjbar A, Arai M and Yunoki S 2018 *Phys. Rev. Mater.* **2** 074002
[110] Kurtoglu M, Naguib M, Gogotsi Y and Barsoum M W 2012 *Mrs Commun.* **2** 133–7
[111] Chakraborty P, Das T, Nafday D, Boeri L and Saha-Dasgupta T 2017 *Phy. Rev.* B **95** 184106
[112] Levitt A, Zhang J, Dion G, Gogotsi Y and Razal J M 2020 *Adv. Funct. Mater.* **30** 2000739
[113] Naguib M, Come J, Dyatkin B, Presser V, Taberna P L, Simon P, Barsoum M W and Gogotsi Y 2012 *Electrochem. Commun.* **16** 61–4
[114] Xie Y *et al* 2014 *J. Am. Chem. Soc.* **136** 6385–94
[115] Yang C, Liu Y, Sun X, Zhang Y, Hou L, Zhang Q and Yuan C 2018 *Electrochim. Acta* **271** 165–72
[116] Dong Y, Wu Z S, Zheng S, Wang X, Qin J, Wang S, Shi X and Bao X 2017 *ACS Nano* **11** 4792–800
[117] Zhang Y, Guo B, Hu L, Xu Q, Li Y, Liu D and Xu M 2018 *J. Alloys Compd.* **732** 448–53
[118] Kajiyama S, Szabova L, Sodeyama K, Iinuma H, Morita R, Gotoh K, Tateyama Y, Okubo M and Yamada A 2016 *ACS Nano* **10** 3334–41
[119] Maughan P A *et al* 2020 *Langmuir* **36** 4370–82
[120] Xie Y, Dall'Agnese Y, Naguib M, Gogotsi Y, Barsoum M W, Zhuang H L and Kent P R 2014 *ACS Nano* **8** 9606–15
[121] Li X *et al* 2020 *ACS Nano* **14** 541–51
[122] Liang X, Garsuch A and Nazar L F 2015 *Angewandte Chemie Int. Edn.* **54** 3907–11
[123] Liang X, Rangom Y, Kwok C Y, Pang Q and Nazar L F 2017 *Adv. Mater.* **29** 1603040
[124] Fang M, Liu X, Ren J C, Yang S, Su G, Fang Q, Lai J, Li S and Liu W 2020 *npj Comput. Mater.* **6** 1–6
[125] Wang Y, Shen J, Xu L C, Yang Z, Li R, Liu R and Li X 2019 *Phys. Chem. Chem. Phys.* **21** 18559–68
[126] Liang J, Sun Z, Li F and Cheng H 2016 Carbon materials for Li-S batteries: functional evolution and performance improvement *Energy Storage Mater.* **2** 76–106
[127] Li Z, Wu H B and Lou X W D 2016 *Energy Env. Sci.* **9** 3061–70
[128] Song J, Zhang C, Guo X, Zhang J, Luo L, Liu H, Wang F and Wang G 2018 *J. Mater. Chem.* A **6** 16610–16
[129] Zhang C, Wu H B, Yuan C, Guo Z and Lou X W 2012 *Angewandte Chemie Int. edn* **51** 9592–5
[130] Zheng G, Zhang Q, Cha J J, Yang Y, Li W, Seh Z W and Cui Y 2013 *Nano Lett.* **13** 1265–70
[131] Cheon S E, Ko K S, Cho J H, Kim S W, Chin E Y and Kim H T 2003 *J. Electrochem. Soc.* **150** A796–A799
[132] Peled E, Gorenshtein A, Segal M and Sternberg Y 1989 *J. Power Sources* **26** 269–71
[133] Park K, Cho J H, Jang J H, Yu B C, Andreah T, Miller K M, Ellison C J and Goodenough J B 2015 *Energy Env. Sci.* **8** 2389–95
[134] Zhao M Q, Liu X F, Zhang Q, Tian G L, Huang J Q, Zhu W and Wei F 2012 *ACS Nano* **6** 10759–69
[135] Wen Z, Hu Y, Wu X, Han J and Gu Z 2013 *Adv. Funct. Mater.* **23** 1005–18
[136] Yin Y X, Xin S, Guo Y G and Wan L J 2013 *Angewandte Chemie Int. Edn.* **52** 13186–200
[137] Ji X, Lee K T and Nazar L F 2009 *Nat. Mater.* **8** 500–6

[138] Li Z, Jiang Y, Yuan L, Yi Z, Wu C, Liu Y, Strasser P and Huang Y 2014 *ACS Nano* **8** 9295–303
[139] Pang Q, Liang X, Kwok C Y and Nazar L F 2016 *Nature Energy* **1** 1–11
[140] Song M K, Zhang Y and Cairns E J 2013 *Nano Lett.* **13** 5891–9
[141] Krishnaveni K, Subadevi R, Sivakumar M, Raja M and Prem Kumar T 2019 *J. Sulfur Chem.* **40** 377–88
[142] Seh Z W, Li W, Cha J J, Zheng G, Yang Y, McDowell M T, Hsu P C and Cui Y 2013 *Nat. Commun.* **4** 1–6
[143] Liang X, Hart C, Pang Q, Garsuch A, Weiss T and Nazar L F 2015 *Nat. Commun.* **6** 1–8
[144] Zhou J, Li R, Fan X, Chen Y, Han R, Li W, Zheng J, Wang B and Li X 2014 *Energy Env. Sci.* **7** 2715–24
[145] Zhang X, Chen A, Zhong M, Zhang Z, Zhang X, Zhou Z and Bu X H 2019 *Electrochem. Energy Rev.* **2** 29–104
[146] Zhao Y and Zhao J 2017 *Appl. Surf. Sci.* **412** 591–8
[147] Sim E S and Chung Y C 2018 *Appl. Surf. Sci.* **435** 210–15
[148] Sim E S, Yi G S, Je M, Lee Y and Chung Y C 2017 *J. Power Sources* **342** 64–9
[149] Zheng J *et al* 2014 *Nano Lett.* **14** 2345–52
[150] Rao D, Zhang L, Wang Y, Meng Z, Qian X, Liu J, Shen X, Qiao G and Lu R 2017 *J. Phys. Chem.* **121** 11047–54
[151] Tang H *et al* 2018 *Adv. Sci.* **5** 1800502
[152] Zhang Y *et al* 2018 *Adv. Funct. Mater.* **28** 1707578
[153] Zhao T, Zhai P, Yang Z, Wang J, Qu L, Du F and Wang J 2018 *Nanoscale* **10** 22954–62
[154] Pourali Z, Yaftian M R and Sovizi M R 2018 *Mater. Chem. Phys.* **217** 117–24
[155] Song J, Guo X, Zhang J, Chen Y, Zhang C, Luo L, Wang F and Wang G 2019 *J. Mater. Chem.* A **7** 6507–13
[156] Du C, Wu J, Yang P, Li S, Xu J and Song K 2019 *Electrochim. Acta* **295** 1067–74
[157] Wang Z, Zhang N, Yu M, Liu J, Wang S and Qiu J 2019 *J. Energy Chem.* **37** 183–91
[158] Zhang H, Qi Q, Zhang P, Zheng W, Chen J, Zhou A, Tian W, Zhang W and Sun Z 2018 *ACS App. Energy Mater.* **2** 705–14
[159] Chen G *et al* 2020 *Energy Storage Mater.* **25** 547–54
[160] Zhuang R, Yao S, Shen X, Li T, Qin S and Yang J 2019 *J. Mater. Sci. Mater. Electron.* **30** 4626–33
[161] Zhou F, Li Z, Luo X, Wu T, Jiang B, Lu L L, Yao H B, Antonietti M and Yu S H 2018 *Nano Lett.* **18** 1035–43
[162] Shi N, Xi B, Feng Z, Liu J, Wei D, Liu J, Feng J and Xiong S 2019 *Adv. Mater. Interfaces* **6** 1802088
[163] Zhao M Q, Xie X, Ren C E, Makaryan T, Anasori B, Wang G and Gogotsi Y 2017 *Adv. Mater.* **29** 1702410
[164] Zheng W, Zhang P, Chen J, Tian W, Zhang Y and Sun Z 2018 *J. Mater. Chem.* A **6** 3543–51
[165] Tontini G, Greaves M, Ghosh S, Bayram V and Barg S 2020 *J. Phys.: Mater.* **3** 022001
[166] Wu Z, Shang T, Deng Y, Tao Y and Yang Q H 2020 *Adv. Sci.* **7** 1903077
[167] Li K *et al* 2020 *Adv. Funct. Mater.* **30** 2000842
[168] Jiang H, Ren D, Wang H, Hu Y, Guo S, Yuan H, Hu P, Zhang L and Li C 2015 *Adv. Mater.* **27** 3687–95
[169] Jariwala D, Sangwan V K, Lauhon L J, Marks T J and Hersam M C 2014 *ACS Nano* **8** 1102–20
[170] Peng L, Zhu Y, Chen D, Ruoff R S and Yu G 2016 *Adv. Energy Mater.* **6** 1600025
[171] Chhowalla M, Shin H S, Eda G, Li L J, Loh K P and Zhang H 2013 *Nat. Chem.* **5** 263
[172] Shi J *et al* 2015 *Adv. Mater.* **27** 7086–92
[173] Das P, Fu Q, Bao X and Wu Z S 2018 *J. Mater. Chem.* A **6** 21747–84
[174] Wu Z S *et al* 2017 *Adv. Mater.* **29** 1602960
[175] Wang J, Liu J, Chao D, Yan J, Lin J and Shen Z X 2014 *Adv. Mater.* **26** 7162–9
[176] Yin S, Tu W, Sheng Y, Du Y, Kraft M, Borgna A and Xu R 2018 *Adv. Mater.* **30** 1705106
[177] Li Y, Wang H, Xie L, Liang Y, Hong G and Dai H 2011 *J. Am. Chem. Soc.* **133** 7296–9
[178] Kong D, Wang H, Cha J J, Pasta M, Koski K J, Yao J and Cui Y 2013 *Nano Lett.* **13** 1341–7
[179] Singh D, Panda P K, Khossossi N, Mishra Y K, Ainane A and Ahuja R 2020 *Catalysis Sci. Technol.* **10** 3279–89
[180] Yu J H, Lee H R, Hong S S, Kong D, Lee H W, Wang H, Xiong F, Wang S and Cui Y 2015 *Nano Lett.* **15** 1031–5
[181] Hou Y, Li J, Wen Z, Cui S, Yuan C and Chen J 2014 *Nano Energy* **8** 157–64
[182] Qu Q, Qian F, Yang S, Gao T, Liu W, Shao J and Zheng H 2016 *ACS Appl. Mater. Interfaces* **8** 1398–405
[183] Zhou X, Wan L J and Guo Y G 2012 *Nanoscale* **4** 5868–71
[184] Wu J, Wang Y, Zhang Y, Meng H, Xu Y, Han Y, Wang Z, Dong Y and Zhang X 2020 *J. Energy Chem.* **47** 203–9
[185] Chaudhari N K, Jin H, Kim B, San Baek D, Joo S H and Lee K 2017 *J. Mater. Chem.* A **5** 24564–79
[186] Sun D, Wang M, Li Z, Fan G, Fan L Z and Zhou A 2014 *Electrochem. Commun.* **47** 80–3
[187] Xu S, Dall'Agnese Y, Li J, Gogotsi Y and Han W 2018 *Chemi. Eur. J.* **24** 18556–63
[188] Byeon A, Zhao M Q, Ren C E, Halim J, Kota S, Urbankowski P, Anasori B, Barsoum M W and Gogotsi Y 2017 *ACS App. Mater. Interfaces* **9** 4296–300
[189] Xie X *et al* 2016 *Nano Energy* **26** 513–23
[190] Ren C E, Zhao M Q, Makaryan T, Halim J, Boota M, Kota S, Anasori B, Barsoum M W and Gogotsi Y 2016 *ChemElectroChem* **3** 689–93
[191] Melchior S A, Palaniyandy N, Sigalas I, Iyuke S E and Ozoemena K I 2019 *Electrochim. Acta* **297** 961–73
[192] Yu P, Cao G, Yi S, Zhang X, Li C, Sun X, Wang K and Ma Y 2018 *Nanoscale* **10** 5906–13
[193] Shen C, Wang L, Zhou A, Zhang H, Chen Z, Hu Q and Qin G 2017 *J. Electrochem. Soc.* **164** A2654–A2659
[194] Liu Y, Wang W, Ying Y, Wang Y and Peng X 2015 *Dalton Trans.* **44** 7123–6
[195] Byeon A *et al* 2016 *J. Power Sources* **326** 686–94
[196] Wu S, Xu R, Lu M, Ge R, Iocozzia J, Han C, Jiang B and Lin Z 2015 *Adv. Energy Mater.* **5** 1500400
[197] Ahmed B, Anjum D H, Hedhili M N, Gogotsi Y and Alshareef H N 2016 *Nanoscale* **8** 7580–7
[198] Zhang C, Kim S J, Ghidiu M, Zhao M Q, Barsoum M W, Nicolosi V and Gogotsi Y 2016 *Adv. Funct. Mater.* **26** 4143–51
[199] Ahmed B, Anjum D H, Gogotsi Y and Alshareef H N 2017 *Nano Energy* **34** 249–56
[200] Luo J, Tao X, Zhang J, Xia Y, Huang H, Zhang L, Gan Y, Liang C and Zhang W 2016 *ACS Nano* **10** 2491–9
[201] Wang F, Wang Z, Zhu J, Yang H, Chen X, Wang L and Yang C 2017 *J. Mater. Sci.* **52** 3556–65
[202] Zhao M Q, Torelli M, Ren C E, Ghidiu M, Ling Z, Anasori B, Barsoum M W and Gogotsi Y 2016 *Nano Energy* **30** 603–13
[203] Lin Z, Sun D, Huang Q, Yang J, Barsoum M W and Yan X 2015 *J. Mater. Chem.* A **3** 14096–100
[204] Zhao S, Meng X, Zhu K, Du F, Chen G, Wei Y, Gogotsi Y and Gao Y 2017 *Energy Storage Mater.* **8** 42–8
[205] Zou G, Zhang Z, Guo J, Liu B, Zhang Q, Fernandez C and Peng Q 2016 *ACS Appl. Mater. Interfaces* **8** 22280–6
[206] Kim S J, Naguib M, Zhao M, Zhang C, Jung H T, Barsoum M W and Gogotsi Y 2015 *Electrochim. Acta* **163** 246–51
[207] Du F, Tang H, Pan L, Zhang T, Lu H, Xiong J, Yang J and Zhang C J 2017 *Electrochim. Acta* **235** 690–9
[208] Zhang C, Kim S, Ghidiu M and Zhao M 2016 *Adv. Funct. Mater* **26** 4143

[209] Huang J, Meng R, Zu L, Wang Z, Feng N, Yang Z, Yu Y and Yang J 2018 *Nano Energy* **46** 20–8
[210] Wang J, Dong S, Li H, Chen Z, Jiang S, Wu L and Zhang X 2018 *J. Electroanal. Chem.* **810** 27–33
[211] Wang Y *et al* 2018 *J. Mater. Chem.* A **6** 11189–97
[212] Chen C *et al* 2018 *Angewandte Chemie Int. Edn* **57** 1846–1850
[213] Wu X, Wang Z, Yu M, Xiu L and Qiu J 2017 *Adv. Mater.* **29** 1607017
[214] Shen C, Wang L, Zhou A, Wang B, Wang X, Lian W, Hu Q, Qin G and Liu X 2018 *Nanomaterials* **8** 80
[215] Ma Z, Zhou X, Deng W, Lei D and Liu Z 2018 *ACS Appl. Mater. Interfaces* **10** 3634–43
[216] Kong F, He X, Liu Q, Qi X, Sun D, Zheng Y, Wang R and Bai Y 2018 *Electrochem. Commun.* **97** 16–21
[217] Zhang Y *et al* 2019 *ACS Nano* **13** 2167–75
[218] Zhang C J, Park S H, Seral-Ascaso A, Barwich S, McEvoy N, Boland C S, Coleman J N, Gogotsi Y and Nicolosi V 2019 *Nat. Commun.* **10** 1–9
[219] Tian Y, An Y and Feng J 2019 *ACS Appl. Mater. Interfaces* **11** 10004–11
[220] Zhang L, Wang K and Zou B 2019 *ChemSusChem* **12** 1612–30
[221] Li H, Lu M, Han W, Li H, Wu Y, Zhang W, Wang J and Zhang B 2019 *J. Energy Chem.* **38** 50–4
[222] Meng J, Zhang F, Zhang L, Liu L, Chen J, Yang B and Yan X 2020 *J. Energy Chem.* **46** 256–63
[223] Liu Y, He Y, Vargun E, Plachy T, Saha P and Cheng Q 2020 *Nanomaterials* **10** 695
[224] Pourali Z, Sovizi M and Yaftian M 2018 *J. Alloys Compd.* **738** 130–7
[225] Zhan C, Naguib M, Lukatskaya M, Kent P R, Gogotsi Y and Jiang D e 2018 *J. Phys. Chem. Lett.* **9** 1223–8
[226] Naguib M, Adams R A, Zhao Y, Zemlyanov D, Varma A, Nanda J and Pol V G 2017 *Chem. Commun.* **53** 6883–6
[227] Li J, Yan D, Hou S, Li Y, Lu T, Yao Y and Pan L 2018 *J. Mater. Chem.* A **6** 1234–43
[228] Guo X, Zhang J, Song J, Wu W, Liu H and Wang G 2018 *Energy Storage Mater.* **14** 306–13
[229] Tao M, Zhang Y, Zhan R, Guo B, Xu Q and Xu M 2018 *Mater. Lett.* **230** 173–6
[230] Guo X, Xie X, Choi S, Zhao Y, Liu H, Wang C, Chang S and Wang G 2017 *J. Mater. Chem.* A **5** 12445–52
[231] Lv G, Wang J, Shi Z and Fan L 2018 *Mater. Lett.* **219** 45–50
[232] Natu V, Clites M, Pomerantseva E and Barsoum M W 2018 *Mater. Res. Lett.* **6** 230–5
[233] Guo Y G 2019 *Nanostructures and Nanomaterials for Batteries: Principles and Applications* (Berlin: Springer)
[234] Er D, Li J, Naguib M, Gogotsi Y and Shenoy V B 2014 *ACS Appl. Mater. Interfaces* **6** 11173–9
[235] Du Y T, Kan X, Yang F, Gan L Y and Schwingenschlögl U 2018 *ACS Appl. Mater. Interfaces* **10** 32867–73
[236] Hou J, Tu K and Chen Z 2016 *J. Phys. Chem.* **120** 18473–8
[237] Demiroglu I, Peeters F M, Gulseren O, Çakır D and Sevik C 2019 *J. Phys. Chem. Lett.* **10** 727–34
[238] Meng Q, Ma J, Zhang Y, Li Z, Hu A, Kai J J and Fan J 2018 *J. Mater. Chem.* A **6** 13652–60
[239] Wang D, Gao Y, Liu Y, Jin D, Gogotsi Y, Meng X, Du F, Chen G and Wei Y 2017 *J. Phys. Chem.* **121** 13025–34
[240] Tang C, Min Y, Chen C, Xu W and Xu L 2019 *Nano Lett.* **19** 5577–86
[241] Aierken Y, Sevik C, Gülseren O, Peeters F M and Çakır D 2018 *J. Mater. Chem.* A **6** 2337–45
[242] Li F, Cabrera C R, Wang J and Chen Z 2016 *RSC Adv.* **6** 81591–6
[243] Çakır D, Sevik C, Gülseren O and Peeters F M 2016 *J. Mater. Chem.* A **4** 6029–35
[244] Zhu J, Chroneos A, Eppinger J and Schwingenschlögl U 2016 *App. Mater. Today* **5** 19–24
[245] Wu Y, Nie P, Jiang J, Ding B, Dou H and Zhang X 2017 *ChemElectroChem* **4** 1560–5
[246] Dall'Agnese Y, Taberna P L, Gogotsi Y and Simon P 2015 *J. Phys. Chem. Lett.* **6** 2305–9
[247] Zhao R, Di H, Hui X, Zhao D, Wang R, Wang C and Yin L 2020 *Energy Env. Sci.* **13** 246–57
[248] Gao X T, Xie Y, Zhu X D, Sun K N, Xie X M, Liu Y T, Yu J Y and Ding B 2018 *Small* **14** 1802443
[249] Lv L P, Guo C F, Sun W and Wang Y 2019 *Small* **15** 1804338
[250] Peng H J, Zhang G, Chen X, Zhang Z W, Xu W T, Huang J Q and Zhang Q 2016 *Angewandte Chemie Int. Edn.* **55** 12990–5
[251] Zhao M Q *et al* 2015 *Angewandte Chemie Int. Edn.* **54** 4810–14
[252] Li B, Zhang D, Liu Y, Yu Y, Li S and Yang S 2017 *Nano Energy* **39** 654–61
[253] Bao W, Xie X, Xu J, Guo X, Song J, Wu W, Su D and Wang G 2017 *Chem. Eur. J.* **23** 12613–19
[254] Bao W, Liu L, Wang C, Choi S, Wang D and Wang G 2018 *Adv. Energy Mater.* **8** 1702485
[255] Chaudhari N K, Jin H, Kim B, San Baek D, Joo S H and Lee K 2018 *J. Mater. Chem.* A **6** 1865–1865